e-Prime - Advances in Electrical Engineering, Electronics and Energy 9 (2024) 100746

Contents lists available at ScienceDirect

e-Prime - Advances in Electrical Engineering, Electronics and Energy

journal homepage: www.elsevier.com/locate/prime

Scientific benchmarking: Engineering quality evaluation of electric vehicle concepts

Nico Rosenberger [*,a], Moritz Fundel [a], Simon Bogdan [a], Lukas Köning [a], Peter Kragt [a], Moritz Kühberger [a], Markus Lienkamp [a]

Technical University of Munich (TUM), School of Engineering & Design, Institute of Automotive Technology, Germany

ARTICLE INFO

Keywords:
Battery electric vehicles
Concept evaluation
Electric powertrain efficiency
Driving dynamics
Comfort
State-of-the-art

ABSTRACT

We present a simulation tool that utilizes advanced modeling techniques to quantify the customer-relevant features of different battery electric vehicles (BEV) concepts. By incorporating comprehensive longitudinal and lateral dynamics analyses, the tool provides an in-depth understanding of passenger vehicle concepts in various driving conditions. Furthermore, the tool emphasizes evaluating comfort, presenting a holistic view concluding into the overall driving experience. Metrics considering the vehicle's packaging are employed to assess the comfort aspects of the concepts. Implementing this simulation tool achieves a more systematic and reliable approach to evaluating BEV concepts. The application based on the parameters of 18 state-of-the-art BEV proved its compliance in the presented categories with the results of physical tests performed by reputable magazines with great experience and comprehensive test protocols. Its academic foundation ensures the utilization of state-of-the-art methodologies and the integration of the latest research findings in vehicle dynamics and comfort. This simulation tool offers automotive engineers, researchers, and industry stakeholders a valuable resource for objectively assessing and benchmarking the performance and comfort aspects of BEV concepts. With its ability to provide accurate evaluations and reasoning for weaknesses, this tool has the potential to significantly contribute to the advancement and optimization of future electric vehicle designs by assessing concepts in early development stages before physical prototypes are available, allowing for cost-efficient modifications.

1. Introduction

According to a study from 2018 [1], 13 % of customers reach their purchase decision for a new vehicle based on car reviews. Including the additional 13 % who base their decision on reviews of friends and internet forums, almost every fourth car is bought due to reviews. A study by *Morning Consult* [2] claims that 60 % of customers withdraw potential decisions after reading poor test results. This highlights the importance of car reviews. Today's arguably most influential car reviews are provided by famous magazines like *Top Gear*, produced by the *BBC*, and *auto motor und sport (AMS)*, published by *Motor Presse Stuttgart GmbH & Co.KG*.

Although most tests provide a wide range of customer-relevant features essential for potential purchase decisions, expensive vehicles tend to score superior in the final evaluation. We believe a significant aspect of optimizing car reviews is considering the recommended retail price (UVP). In Fig. 1, each blue point represents a BEV's individual evaluation score of the BEV specific test procedures from *AMS*, the so-called *E-Auto Supertest* over its UVP. The overall results strongly depend on the vehicles' price, with the two most expensive vehicles being rated best, whereas the cheapest is rated worst. It is also shown that most vehicles in similar price categories reach similar results. However, our study aims to reach a vehicle ratingindependent of their UVP but instead focuses on the variances from the shown linear trend line (orange). It appears that these variances are more interesting when evaluating the engineering quality, as shown in a superior vehicle (green arrow) and a inferior vehicle (red arrow) which is not yet elaborated in car reviews.

In addition to the presented UVP dependency, the results in specific procedures are compared to their contenders, which results in vehicles with a later start of production (SOP) being evaluated more competitively than earlier concepts. This also highlights the importance of individual vehicle evaluation. Comparing a vehicle's test results to potential results, which can be reached with the given vehicle concept,

* Corresponding author.
E-mail address: nico.rosenberger@tum.de (N. Rosenberger).

https://doi.org/10.1016/j.prime.2024.100746
Received 3 May 2024; Received in revised form 27 July 2024; Accepted 21 August 2024
Available online 23 August 2024

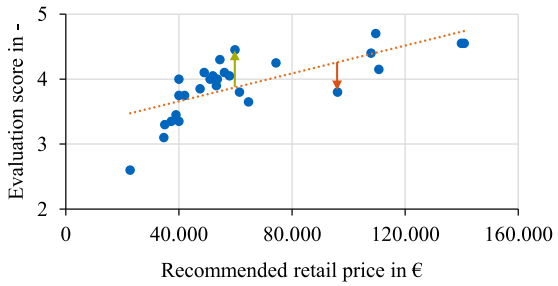

Fig. 1. Current results of the *AMS E-Auto Supertest* with the blue points representing the test vehicles and the orange trendline the dependency on the UVP [3].

more unbiased evaluations are reached. These evaluations emphasize the engineering quality against state-of-the-art BEV concepts.

Literature research yields information for BEV data on component and for basic evaluations also on vehicle level: On component level, Moment et al. [4] observed the efficiency map of the electric machine of a Chevrolet Bolt. Sarlioglu et al. [5] extend the analysis of the electric machine by including power electronics and batteries. Unfortunately, these observations are not transferred to effects on vehicle level. Kovachev et al. [6] investigated the powertrain on vehicle level by comprehensively analyzing the battery pack regarding safety, but no performance tests were performed.

Oh et al. [7] provided the most comprehensive data, in which 383 vehicles (including 27 BEVs) were tested. The advanced vehicle testing and evaluation study (AVTE) [8], a collaborative effort of different American institutions (led by the National Energy Technology Laboratory (NETL)), investigated the performance of 30 vehicles on both component and vehicle level. The data for this study has been gathered between 2011 and 2018. Grunditz et al. [9] presents a comprehensive performance analysis including energy consumption, range, acceleration time, and top speed based on 40 BEV. Wassiliadis et al. [10] offer comprehensive component and vehicle data of a current mass-series electric vehicle (Volkswagen ID.3 Performance from 2020), which focuses on costumer-relevant features such as range, efficiency, and lifetime. Our research group continued this work and analyzed the Tesla Model 3 SR+ from 2020, focusing especially on vehicle level [11]. All the studies highlight the effort of conducting data on a physical level with actual test vehicles to provide such analysis.

Evaluation based on simulation models is often referred to as so-called digital twins. The importance of applying simulation models to the development process in the automotive industry is described by Piromalis et al. [12]. They reach for quicker results and optimize the component design in many aspects of its development process. Further studies [13–15] present the application fields of digital twins mainly in component design, monitoring and estimation of the operation status, and error detection. The overall vehicle concept analysis and evaluation, especially compared to current state-of-the-art competitors, is yet to be established. Our aim is to base our analysis on simulation results of vehicle models so that results can be provided shortly after releasing new BEVs or even before physical prototypes are available.

1.1. Contributions

This study presents an approach to objectively evaluating current electric vehicle concepts independent of their UVP. This study is based on the work of Nicoletti [16], who provided a tool for designing electric vehicle concepts, translating performance requirements as inputs into electric powertrain architectures. In this study, we present a tool that works vice versa, obtaining performance characteristics as outputs. This tool is supposed to highlight the engineering quality by evaluating BEV concepts against themselves and not against each other. The real vehicles are evaluated in developer-relevant features specifically and restricted to BEV-relevant features regarding performance and comfort. Determining possible optimization potentials in different categories, the vehicles are in a second step compared against each other. Finally, these results will be compiled as an Engineering score. The objectives of this article can be summarized as follows:

- Conceptual delimitation of a digital twin and our reference model determined through different levels of parameters.
- Design of a battery electric vehicle architecture determining the vehicle's potential packaging based on the official dimensional chains and the design of powertrain components.
- Implementation of a longitudinal dynamics model identifying potential performance characteristics regarding acceleration time and energy consumption applying official test cycles.
- Implementation of a lateral dynamics system guaranteeing a holistic evaluation considering lateral performance characteristics potentially affecting longitudinal performance results.
- Elaboration of the objective and cost-independent evaluation scheme and finally presenting the results of state-of-the-art electric vehicle concepts.
- Open access to a simulation tool, which will be published alongside this article, available via FTMGithub, allowing manufacturers to include their own vehicle concepts into our tool and evaluate their concepts against the current BEV.

1.2. Layout

This article is structured as follows: Starting with explaining the overall concept, the design or modification of the simulation tool is described in Section 2. Inputs are categorized, and we will show how unknown data is not recorded but bypassed. After the overall concept, the single implemented modules that later evaluate the vehicles are presented as comfort criteria through the packaging analysis in Section 3, and the performance criteria in Section 4. Before we present our results, we demonstrate our evaluation scheme in Section 5. Finally, we validate our model by discussing the results that we achieved. Lastly, Section 6 concludes the Benchmarking of BEV concepts based on simulations.

2. Digital reference model development

The benchmarking tool consists of a simulation model that creates a digital reference model of an existing BEV considering both volumetry and gravimetry of the installed components and estimates its resulting dynamics. The design of the reference model is followed by an evaluation scheme for comparing the real vehicle's characteristics with the simulated ones of the reference model. Fig. 2 illustrates the benchmarking tool's process, including the initialization and simulation of the reference model and the final evaluation with the real vehicle data. The overall concept is briefly discussed in this section, with a more detailed look at the simulation and the evaluation in the respective sections, as indicated by the orange numbers in the upper right corner of the presented boxes.

To set up the reference model, we considered the same simulation approach as Nicoletti [16] by using only a limited set of input parameters. Real vehicle parameters define the basic structure of the reference model to guarantee comparability between the real vehicle and the reference model. Unknown parameters are computed as average or regression-based values using a database containing a wide variety of more than 2000 vehicles. Various manufacturers, vehicle classes and body shapes, technical implementations of the drive train, and prices are included in this database. Therefore, our reference model does not correspond to a digital twin. Instead, with the average parameters, the reference model represents a mean vehicle based on the current state-of-the-art of the automotive industry. This state-of-the-art is defined by the parameters derived from the database. Freely selectable

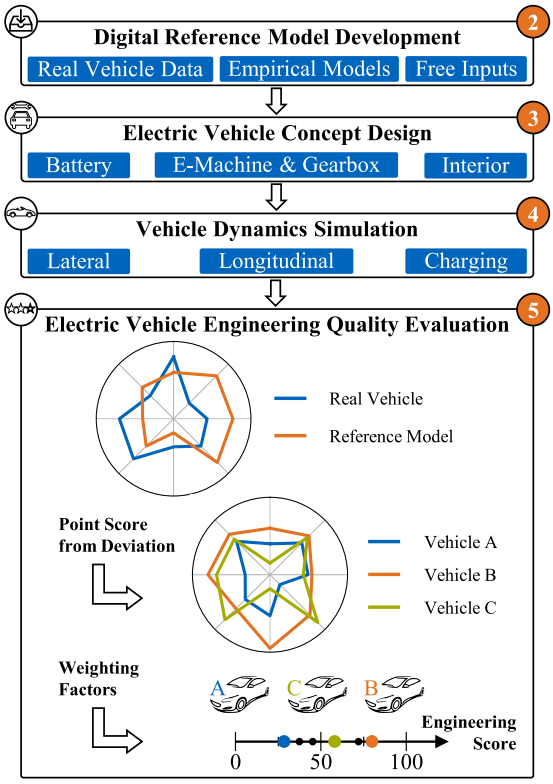

Fig. 2. Overall concept of the presented methodology with reference to their respective sections.

parameters allow defining certain inputs like the machine efficiency map, the driving cycle, and the charging curve as individual state-of-the-art. A brief overview of the architecture of the reference model and the setup of required real input parameters, statistically derived parameters, and freely selectable ones is presented in Sections 2.1 and 2.2.

After the initialization of the reference model, its packaging is estimated. This design process begins with the simulation of the interior of the vehicle. Dimensions inside the passenger cabin are calculated using official standards provided by the Society of Automotive Engineers (SAE). Secondly, volumetric simulations of the electric machine(s), the gearbox, and the high-voltage battery are executed. Lastly, the vehicle concept design is completed by calculating the reference mass and applying the methods and rules developed by Nicoletti et al. [16,17].

Based on the volumetric and gravimetric design of the reference model, its dynamics are simulated. The longitudinal simulation considers the acceleration, energy consumption, and electric range according to a selected driving cycle. The lateral dynamics are taken into account by analyzing the *18m slalom maneuver*. The dynamic simulation concludes with the estimation of the charging time.

Finally, the simulated characteristics of the reference model and the ones of the real vehicle are evaluated. Hence, the percentage deviation between simulation and reality in multiple customer-relevant criteria is transformed into an individual point score. This individual point score enables the evaluation of the design of the components and dynamics of the real vehicle. The weighted summary of the individual point scores leads to the final Engineering score for each vehicle.

2.1. Vehicle architecture

The vehicle architecture of the reference model requires four different features described by Nicoletti et al. [18] containing the dimensional concept, dimensional chains, powertrain topology, and component modeling.

2.1.1. Dimensional concept

The dimensional concept defines the vehicle dimensions and determines the geometrical constraints of the vehicle package [16,18]. The dimensional concept is based on the SAE standards. The most important dimensions are described in the SAE J1100 [19], which are classified into length (L), height (H), and width (W). A reference coordinate system enables the definition of the exact components' position. This coordinate system is placed according to the ISO 4130 standard in the center of the front axle, with the X-dimension increasing towards the longitudinal end of the vehicle and the Z-dimension along the vehicle's height [20]. The dimensional concept consists of three sub-characteristics, all shown in Fig. 3, including the reference coordinate system.

The exterior concept contains the external dimensions of the vehicle. The interior concept refers to the required space of the driver and passengers [21]. Therefore, conceptional human dimensions are defined with a two-dimensional manikin [22]. Reference points are necessary to position the manikin adequately inside the passenger cabin. The Seating Reference Point (SgRP) ① indicates the position of the hip. The heel position of the driver and the passengers in the second seat row is defined as Acceleration Heel Point (AHP) ② and Floor Reference Point (FRP) ③, respectively [19]. Finally, the sight and trunk concept deals with the driver's field of vision and the available space to store luggage [16].

2.1.2. Dimensional chains

Dimensional chains are defined as a succession of elements in which the next item directly follows the previous one [23]. Felgenhauer et al. [24] specify the dimensional chain as the sum of the components' lengths and their distances along a respective coordinate direction. Dimensional chains are used to identify the available space and the necessary dimensions of various components like the battery installation space [25]. For example, Fig. 3 shows the entire vehicle length as the sum of the wheelbase L101 and the front and rear overhang L104 and L105.

2.1.3. Drive topology

The topology combines the general decision for a certain powertrain concept with its components' design and geometrical positioning [16,26]. The powertrain consists of the traction battery, the power electronics, the electric machine, the gearbox, and the charger [27]. This scope will distinguish between battery, electric machine, and transmission topology.

The battery topology comprises the integration principle and its shape [27]. The integration principle defines the battery's position in the underfloor and its effects on the dimensional concept [16]. Both SgRP-1 and SgRP-2 are necessary to differentiate between the integration principles. For a highfloor principle, the battery is positioned between the vehicle ground and the interior compartment. Therefore, it affects the position of the seating reference points, which must be shifted upwards [27]. In a lowfloor vehicle, the battery does not affect the seating reference points because the battery is placed in the tunnel and underneath the seats [16]. Additionally, in mixedfloor vehicles, not all seating reference points are affected by the battery, making this

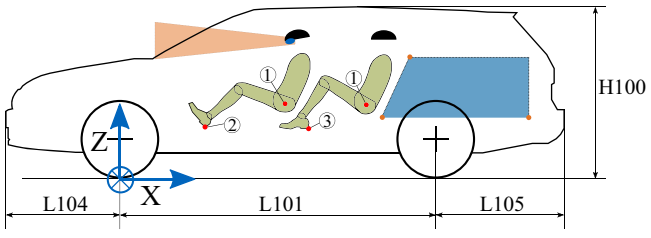

Fig. 3. The three features of the dimensional concept.

principle a hybrid between high- and lowfloor vehicles [27]. Regarding the battery shape, four different basic shapes are described. While the rectangular and drop-shape form is mostly used in highfloor vehicles, lowfloor vehicles use a cross- or T-formed shaped battery [27].

Electric machines provide the necessary torque for the motion of the BEV. Since most BEV use a central machine topology, only this is implemented in the tool. The central machine propels an entire axle with additional components such as the gearbox, differential, and driveshafts [28]. Central machines can be classified by the relative position of the axis, in front, behind, or coaxial to the corresponding axle [29].

Since we only consider central machines, a gearbox adapts the high engine speed to the lower speed of the wheels [30]. BEV mostly use single-speed, two-staged gearboxes due to their efficiency, simplicity, and cost savings [16,31]. Gearboxes can be subdivided into parallel or coaxial gearboxes based on the alignment of the input and output shafts. For our reference model, the design of the simulated gearbox follows an approach introduced by Nicoletti et al. [29].

2.1.4. Component models

A component model is used to evaluate the volume and mass of a certain component [16]. In the presented tool, mostly semi-physical and empirical models are used. Empirical models use statistical methods based on measured data, whereas semi-physical models combine those statistical methods with physical correlations [16]. An example of such a semi-physical approach is the volumetric simulation of the electric machine presented in Section 3.2: The scaling of the machine is based on physical law, while the housing thickness is determined using empirical factors. Various input data are required to create those empirical factors, either based on the manufacturer‘s data or databases and standards. An overview of all used empirical models is given in Section 2.2.2.

2.2. Parameters of the reference model

To calculate the digital reference model of a specific vehicle, various input parameters are required. The input parameters can be subdivided into three different types. Firstly, real data values of the BEV to be digitally mapped are required. Accordingly, these are different for all vehicles under investigation. Secondly, there are parameters derived from empirical models. Thirdly, some parameters can be freely chosen by the user. The last two types of parameters allow the calculation of the reference model based on the state-of-the-art instead of a digital twin. In contrast to the real vehicle inputs, those parameters follow the same calculation rule for each simulated vehicle.

2.2.1. Parameters of the real vehicle

Real vehicle parameters define the frame of the reference model. This ensures that the reference model is a simulative representation of the real vehicle. Some of these parameters can be found in publicly accessible online databases like the ones of the Allgemeiner Deutscher Automobilclub (ADAC) or the ev-database [32,33]. A deeper insight into the vehicle’s inner structure is required for other parameters. Those can be determined using three-dimensional vehicle models, for example, provided by A2Mac1 [34].

The starting point for designing the reference model are the external dimensions of the real vehicle. Its height H100, width W103, and wheelbase L101, define the boundaries of the available space. Additionally, the vehicle’s frame form influences the mass of the vehicle. The turning circle and possibly integrated rear-axle steering affect the wheelhouses and, therefore, the installation space for the battery. Finally, the real ground clearance is necessary for the design of the passenger cabin.

Additionally, several interior dimensions are required for the simulation. As there is a wide variation in the real implementation of the seating height H30-1 [35], this dimension is taken from the real vehicle. Since the dimensions at the rear seat cannot be estimated properly by a manikin, the seat height H30-2 and the headroom H61-2 are taken from the real vehicle. To calculate the trunk volume, three inputs of the real vehicle are necessary: H252 describes the vertical distance between the ground and the lowest point of the trunk, H297-2 depicts the trunk’s height, and finally, the outline of the trunk volume.

Real vehicle information is also required to map the electric machine and gearbox topology. This includes the number of electrical machines and the driven axle(s). Options for the machine types include Induction Machine (IM), Permanent Magnet Synchronous Machine (PMSM), and Separately excited Synchronous Machine (SSM). For designing the electric machine(s) we use a scaling approach. The maximum torque and power are preconditions for the scaling. The real gear ratio is required to estimate the size of the gears, shafts, and bearings.

To simulate the battery, information about the cells, the available installation space, the position within the vehicle and information about the electronic configuration is needed. Cell information includes the cell type (pouch, cylindrical, prismatic as the current state of the art [36]) and its height. Secondly, the integration principle and the different areas filled with battery cells (Fig. 4) must be defined. Thirdly, the real distance between the electric machine and battery or, in the case of a non-driven axle, the distance between axle and battery for both axles is required. Furthermore, the relative position of the battery to the rear tires is needed to calculate the battery width W_{batt} (Fig. 5). Lastly, the electronic configuration of the simulated battery is defined by using the real pack configuration of serial and parallel cells.

Computing the battery’s length requires the dimensions of the wheelhouses. For this purpose, we use the real tire dimensions for both axles according to the ISO metric codes containing the tire width and the diameter of the tire and rim. The front steering angle can be calculated based on the tire dimensions, the turning radius, and the rear steering angle. Subsequently, the wheelhouse dimensions are computed following the approach of Nicoletti et al. [37]. Additionally, the ISO metric codes of the tires used by *AMS* for their lateral dynamics testing are required to guarantee the same baseline for the simulation and the real testing.

The charging time estimation mostly depends on the maximum and average charging power. The real capacity is required to conduct an independent charging time simulation instead of the simulated one. In addition, the cathode material is a relevant input. Considered are only Lithium Iron Phosphate (LFP), Lithium Nickel Cobalt Aluminum Oxide (NCA), and Lithium Nickel Manganese Cobalt Oxide (NMC) cathode materials since these are the most widespread in vehicle batteries [38].

Lastly, the real vehicle’s mass is required. Although a gravimetric simulation is conducted, some components, like the shock absorber or the brakes, are designed with the real vehicle mass to better represent the real components. Additionally, for executing the gravimetric simulation the mass distribution and the material of exterior components like the door and hood (steel or aluminum) are required.

To conduct the benchmark analysis the comparative values from the

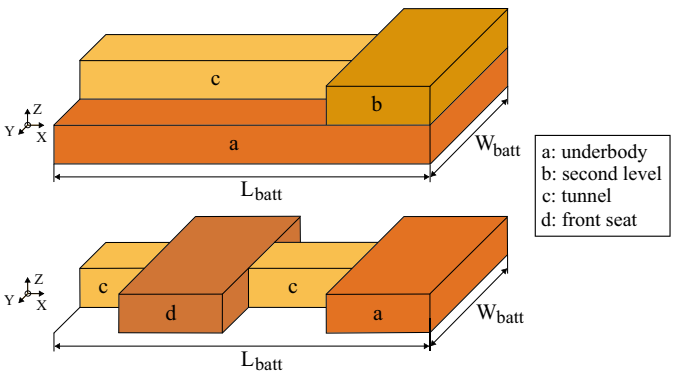

Fig. 4. Considered battery areas for highfloor (top) and lowfloor vehicles (bottom).

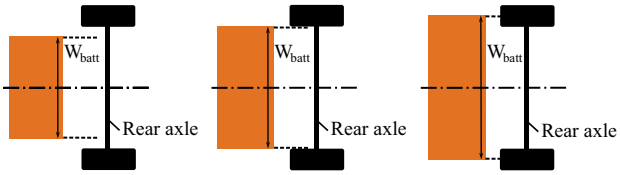

Fig. 5. Sizing of the battery pack in lateral direction.

real vehicles are also stored in the same table. Section 5.1 gives a detailed explanation of those values.

2.2.2. Parameters through empirical models

Since only a few real vehicle parameters are used to create the reference, many other parameters must be estimated with statistical models. Data sets of different vehicles are required to use the statistical methods. Those data sets are stored in a database like the one presented in [18]. All non-predefined but necessary vehicle parameters can be calculated using this database. Adding new vehicles into the database varies the results of the statistical methods and therefore prevents the database from data-aging [16]. A differentiation is made between three different types of obtaining certain parameters from the database.

Firstly, fixed parameters are defined once and do not change by adding new vehicles to the database. These parameters are either predefined by standards or cannot be explicitly determined for a certain vehicle. For instance, the manikin's thigh length used for the dimensional concept is defined in the SAE J826 [39] or the efficiencies of the gearbox origin from various publications (Table 1).

Secondly, unknown parameters can be determined using data from several databases. If these do not correlate with other parameters stored in the database, they are used as constant average values. The mean parameters are calculated using statistical processing like the Kolmogorov-Smirnov test and subsequent elimination of statistically irrelevant parameters.

Thirdly, a linear regression determines the simulated parameter if there is a dependency between the parameter and other characteristic values. A linear regression describes a linear dependency between independent input variables and the dependent output variable of a system. To statistically validate the linear regression model, the F- and t-test are conducted [40,41].

2.2.3. Freely definable parameters

Three other necessary design variables can be specified by the user. These include the driving cycle, the characteristics of the electric machine, and the charging curve.

For simulating a BEV's energy consumption, the standardized Worldwide harmonized Light vehicles Test Procedure (WLTP) cycle [42] is considered since this is the current standard for the determination of consumption in the European Union. Additionally, for estimating the vehicle's range, the ADAC-Ecotest [43] is used. The Ecotest consists of a complete WLTP cycle and an additional highway cycle. On the one hand, using the Ecotest avoids the repeated usage of the same cycle for two evaluation criteria. Since the presented tool calculates the range based on the division of capacity and energy consumption, the Ecotest offers good comparability due to the same calculation. On the other hand, the Ecotest provides comparative values determined by an independent organization during their BEV-tests.

The characteristic of an electric machine consists of the torque over speed curve and the efficiency map. The efficiency map assigns an efficiency to each operating point of the electric machine consisting of the torque and the corresponding speed [44]. Three different machine characteristics are provided one for each of the aforementioned types of electric machines [45].

In the context of the tool, a charging curve is defined as the charging power over the battery's actual state of charge (SOC). For fast charging, we only consider the area between 10 % and 80 % SOC as also contemplated by the P3 Charging Index [46] or the ev-database analysis [33]. Since the charging curve differs for various models, we introduced four generic charging curves representing various charging behaviors to fulfill the tool's overall objective of developing a non-vehicle-specific simulation approach. These generic curves represents a standardized relation between charging power and SOC and is afterward scaled up to the maximum charging power of the real vehicle.

3. Electric vehicle concept design

At the beginning of the vehicle design process, the challenges of installation space and its utilization, the packaging, get a particularly intriguing aspect. Since the simulation model designs a vehicle from scratch, we present the procedure for battery modeling, drivetrain sizing, and interior design based on the previously presented dimensional chains in this section.

3.1. Determination of the battery installation space

The battery is the largest component in BEV, so it is dimensioned first. Based on the integration principle, the battery consists of various individual regions. These are visualized in Fig. 4 considering all possible areas for highfloor vehicles on the top and lowfloor vehicles on the bottom. The horizontal, lateral and vertical dimensions of the battery are shown.

In highfloor vehicles, the battery is implemented as a cuboid and fills the area between vehicle ground and interior. In the following, this area is called the underbody. Additionally, cells can be placed on top of the underbody, filling the vehicle tunnel and the area underneath the second seat row. The Polestar 2 is an example of such an implementation [47]. On the contrary, lowfloor vehicles do not use the whole underbody to store battery cells. Instead, the volume of the underbody is reduced and describes only the area underneath the second seat row. Like highfloor vehicles, a second pack of cells can be positioned atop the underbody. In this study, the area is assumed to cover the entire W_{batt}. Finally, the tunnel offers additional space for further cells. However, in lowfloor vehicles, the tunnel is placed at the same height as the underbody while, in highfloor vehicles, it is placed on top of the underbody.

3.1.1. Dimensioning the vertical space of the battery

The approach determining the battery parameters in vertical and horizontal directions is based on [27]. Modeling the battery height, only one cell is assumed to be installed in the vertical direction. The height is significantly influenced by the height of a cell, which is specified as a direct input parameter. An average value is added considering the module height and the distance between the module and the housing. Furthermore, the battery housing is considered by using average parameters for the thickness of the base, the lid of the housing, and the cooling structure.

3.1.2. Dimensioning the horizontal space of the battery

In the horizontal direction, the battery installation space is restricted by the front and rear axle units containing chassis components and motor-gearbox units. In addition, the wheel arches on all four tires show a considerable restriction. For each installed drive unit, the arrangement of it in comparison to the axle is examined (Section 2.1.3). The battery length L_{batt} is determined with the shortest available distance, and the real safety distance between the battery and the drive unit is added. Additionally, it is checked whether the wheel arch influences the installation space in the horizontal direction of the battery. It is defined by the tire width, the steering angle, and an average wheel arch width. Therefore, the battery is placed within these limits. An exception is a variant in which battery space between the wheel arches is planned from the start [16], where additional installation space for the battery is created in the horizontal direction.

3.1.3. Dimensioning the lateral space of the battery

W_{batt} is modeled with a correction factor considering the relative position of the real vehicle battery. Depending on the manufacturer's implementation, the width is either smaller than the distance between the tires on the rear axle, as wide as the inside of the tire, or larger than this dimension (Fig. 5). Depending on the variant, W_{batt} of the reference model can be calculated with a defined factor, which reflects a relation between vehicle width and W_{batt}. The factor is determined for each category based on the existing data in the database and averaged. Besides the three methods presented, an additional factor for conversion design vehicles is modeled, as the previous categorization did not show a correlation for this design approach.

3.1.4. Defining the final battery installation space

Given L_{batt} and W_{batt}, the individual dimensions for the installation space are computed. The rectangular underbody of highfloor vehicles is defined by L_{batt} and W_{batt}. For the length of the underbody of lowfloor vehicles, the approach stated in [16] is used. The length depends on the position of the SgRP-2 and the empirically calculated seat length. If the second level is filled, this method can be applied similarly to all integration principles. A similar concept is used for the area below the front seats. The position of the SgRP-1 and an empirically derived front seat length define the length of this area. To dimension the tunnel, the approach described in [16] considers the lateral position of the SgRP-1 and the empirically derived seat width. The presented method enables us to simulate the battery dimensions of lowfloor vehicles such as the Opel Mokka e with the same accuracy as highfloor vehicles.

3.1.5. Filling the installation space with cells

To provide sufficient energy for the operation of a BEV, the installation space, considering all available areas, must be filled with cells. In our approach, the real pack configuration, consisting of parallel and serial cells, is used as an input. Thus, the reference model features the same number of cells and battery voltage as the real vehicle. Further core parameters are the cell dimensions length, width, and height. Since the height is taken as an input parameter, the filling process is conducted in a two-dimensional space. Averaged package factors increase the cell dimensions in both directions, considering additional components like cable and cooling systems [16]. The filling process aims to maximize the cell dimensions while ensuring the given pack configuration.

The iterative process fills each possible area with an integer number of cells. Since there is a geometric dependency between the length and width of cylindrical cells, only one degree of freedom exists. Therefore, the maximal diameter of these cells is estimated. Due to an additional degree of freedom for pouch and prismatic cells, further input is required. We specify an interval for the cell's width using the minimal and maximal width from all cells in the database as boundaries. For pouch and prismatic cells, the combination of length and width is estimated. The iteration terminates as soon as the maximum cell dimensions are found.

Based on the cell dimensions, the calculation of the battery's capacity is possible. It includes the determination of the cell volume considering only the active cell material. Subsequently, the gross battery capacity is the product of the individual cell volume, the volumetric energy density, and the total number of cells. The average energy density is calculated for each cell type. To increase the longevity of the battery, the gross capacity in BEV is not fully used to provide the driving power [9]. Therefore, an empirically derived mean factor estimates the usable net energy based on the gross capacity.

3.2. Determination of the electric machine and gearbox

For the volumetric design of the electric machine, a scaling approach is implemented. The aim is to geometrically modify a known reference machine so that it coincides with one of the characteristic data of the real installed machine [48].

The scaling approach was presented by Pries and Hofmann [49] and fulfills the electromagnetic and thermal dynamics. To align the torque of the scaled, simulated machine exactly to the torque of the real machine T_{real}, a scaling factor λ is calculated using Equation 1.

$$\lambda = \sqrt[3]{\frac{T_{real}}{T_{reference}}} \tag{1}$$

This scaling factor is then applied to calculate the rotational speed and the resulting scaled power. Since the scaling factor does not influence the efficiency map, the scaled map corresponds to the one of the reference machine. Hence, the efficiencies do not change, only the corresponding operating points shift due to the scaling factor. To take the geometric differences of the scaled machine into account, the scaling factor is multiplied by the diameter of the reference machine, which yields a scaled diameter. Based on the scaled diameter, the length and volume of the electric machine can be estimated using the approach described in [16].

In addition to the electric machine, the transmission is also modeled concerning the installation space and components. The method is adopted from [29] and designs a single-speed gearbox based on the required properties, whereby the executed gearbox design is adopted from the real vehicle.

3.3. Determination of interior dimensions

The interior concept is developed following the sizing of the battery and drive unit. In addition to the front and rear seating rows, the vehicle design includes the trunk as another important comfort feature.

3.3.1. Sizing the vertical interior space

The modeling of the available interior space in the vertical direction is based on the methods of Nicoletti et al. [50]. Still, some adjustments are made to enable benchmark studies. H100 is crucial for the interior. With H100, the battery height, the real ground clearance H156, and the battery integration principle, the interior height is determined according to Fig. 6. The roof thickness is determined using an average parameter while considering an optional glass roof. The dimensions H30-1, H5-1 and H61-1, the latter being angled 8 degrees following the SAE J1100 [19], are determined using predefined dimensions of a 95th percentile manikin according to the SAE J1052 [51] and the reference points ①, ② and ③. The procedure results in specific dimensions for the front seats, which can be compared and evaluated with the real vehicle's.

As manufacturers rely on different solutions for designing the rear row of seats [35], the H61-2 dimension is given by the real vehicle. Hence, the position of the SgRP-2 can be computed considering the roof thickness and an offset caused by the lower position of the roof at the second seat row [16]. To include the headroom of the second row in the benchmark analysis without real vehicle values, a further 95th percentile manikin and a similar dimensional chain to the front row (H100, H30-2, thickness of roof) is used based on [50].

Determining H252, a distinction is made whether a drive unit is installed at the rear axle. For vehicles with a drive unit at the rear of the vehicle, its vertical height is determined and combined with an empirical value considering the distance between trunk and drive unit.

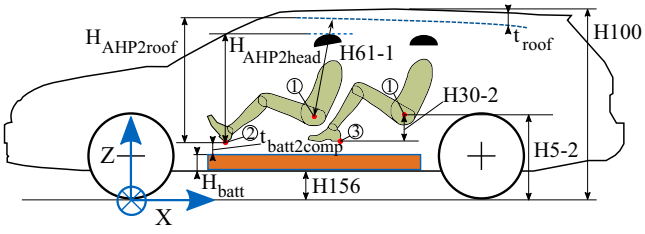

Fig. 6. Available vertical space in the interior.

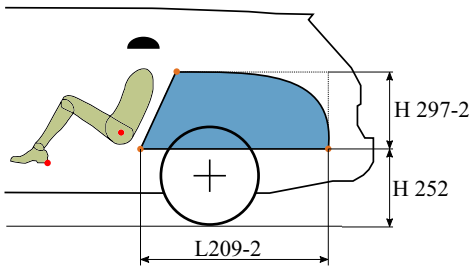

Fig. 7. Side view of modeling the trunk.

Otherwise, the real H252 is used. The height of the trunk corresponds to the height of the rear seat [19]. Since this height is not modeled, the shoulder height of the manikin in the second row is used as the reference point. When modeling the side surface of the trunk, a simple prismatic-shaped area does not adequately reflect reality. Therefore, the vertical contour of the trunk is determined using the profile of the real vehicle, and the volume is adjusted accordingly (Fig. 7).

3.3.2. Sizing the horizontal interior space

For the horizontal simulation of the interior space, a separate method is implemented for the front and rear seats, following [18]. For the dimensions of the front passengers, the length measure L53-1 is determined using the on the SgRP-1 placed 95th percentile manikin and the real H30-1 (Fig. 8). With L113, this results in the total horizontal space for the front passengers, L99-1.

The measurement of the distance from the rear axle to the SgRP-2 (L115-2) differs significantly depending on the body design used. Thus, we use a regression based on L101 and L113. Using L115-2, the horizontal distance between the two SgRP's L50-2 and consequently the legroom L53-2 via the wheelbase and the FRP in the second seating row are determined.

The length of the trunk is determined between the front and rear points of the trunk floor. The back of the rear seat represents the front boundary. It can be calculated by using the SgRP-2 and adding the distance to the seat cushion and the thickness of the seat cushion itself. These parameters are mean values taken from the database. With the seat angled at 25°, following the SAE J4002 [52], the intersection of the trunk floor and the back of the seat can be determined. The endpoint of the trunk is calculated using averaged parameters for the distance between the trunk and the rearmost point of the vehicle as well as L105.

3.3.3. Sizing the lateral interior space

Using the method of Mau and Venhovens [53], a fixed parameter for each vehicle's body design is set as the distance between the elbow of the manikin and the inside of the door. The interior width is resolved using the vehicle's width and a fixed parameter considering the seat width.

The trunk width is estimated using the position of the dampers on the rear axle. With the determined innermost point of the damper, an empirical distance between the shock absorber and the trunk derived from the database is added. It defines the distance of the trunk to the center of the vehicle and calculates the entire trunk width W201 by doubling the result.

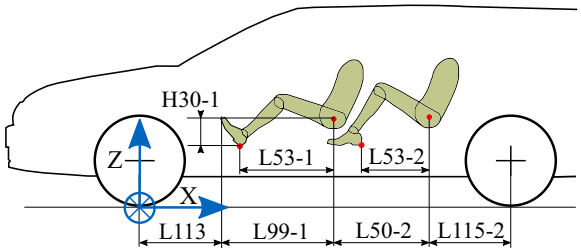

Fig. 8. Available horizontal space in the interior.

3.3.4. Results of the comfort criteria

One important feature of a vehicle concept is the headroom of the passengers in the front and rear seating rows. The relevant measures within the interior concept are H61-1 and H61-2.

For the front seats, the simulation provides an average deviation between real and simulated H61-1 of -0.77 %, where the individual results for each vehicle can be seen in Fig. 9. A positive deviation indicates that the simulation result exceeds the real vehicle's, while a negative deviation signifies the converse. Specifically, in the context of H61-1, a positive deviation suggests that the reference vehicle affords greater passenger vertical space. This assessment is adapted according to the criterion being analyzed.

Reasons for deviations of the headroom can be found in the entire dimensional chain consisting of the vehicle height, the position of the AHP, the H30-1 dimension, and the thickness of the roof. The position of the AHP, for example, depends on the battery height and the distance between the battery and the interior, the latter parameter varying depending on the manufacturer and being used as a fixed parameter. The H30-1 is coupled in a dimensional chain with the legroom of the front passengers. In the case of the Renault Zoe, this coupling results in larger deviations, as its seating position is comparatively upright, and the real H30-1 dimension is significantly higher than the ones of the competition [54]. As a result, the simulated H61-1 is higher than the real one. Therefore, the reference model of the Renault Zoe can provide +11 % more headroom than the real vehicle. Regarding the position of the AHP, relatively large deviations can be found in the vehicles with an EV-only platform from Volkswagen (MEB). This difference is due to differences in the distance between the battery and the interior [34].

The headroom of the rear seat is described with the H61-2 parameter. On average, the results show a deviation of +6 %. Due to the method for the calculation of the H61-2 dimension, which uses a 95th percentile manikin in the rear seating row, the deviations are positive and the same for the majority of the analyzed vehicles. Only in a few cases, the vertical space for a 95th percentile manikin is limited in the second seating row, resulting in a negative deviation. Furthermore, deviations in this area can, for example, relate to the average roof thickness following the generalized approach. The H61-2 of the Fiat 500e is simulated higher than the real vehicle. Due to the design, the manufacturer reduces the measure to achieve a tolerable seating position [55]. A different example of a negative deviation is the BMW iX. The simulated headroom is smaller than the real one. This deviation

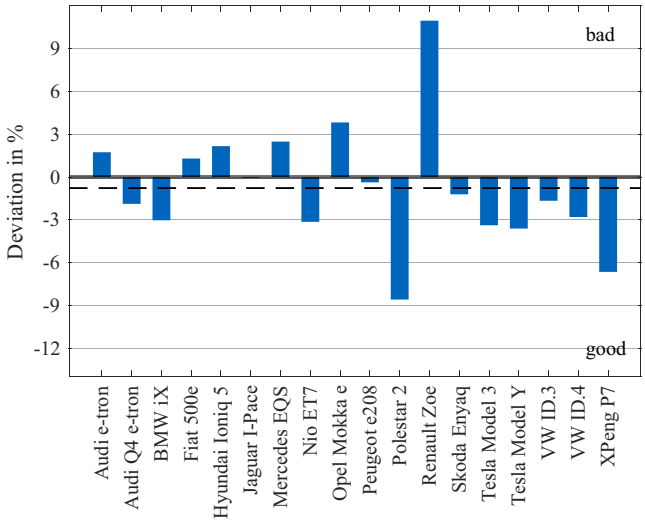

Fig. 9. Deviations in H61-1 for all 18 vehicles.

correlates to reviews of that car, where one mentioned positive aspect of the vehicle is the big dimensioned headroom space in the second row [56].

In addition to the headroom, the legroom L50-2, which analyses the horizontal design, is another evaluated comfort measure. An average deviation of +5 % is shown in Fig. 10.

The result of the measure is influenced separately by several elements. One of these parameters is the position of the SgRP-1, which influences the legroom significantly. One distinguishing example is the Hyundai Ioniq 5, which shows a large deviation in the L99-1 dimension following the positioning of the SgRP-1 and a bigger H30-1 compared to the competition [34]. Similar patterns are evident within the Jaguar I-Pace. On the other hand, for vehicles based on the MEB platform, such as the Audi Q4 e-tron, the SgRP-2 of the real vehicle is moved backward [34]. That measure results in more usable legroom in the rear of the vehicle [57].

Modeling the trunk with a combination of direct inputs, such as the trunk contour, and simulated parameters, such as the trunk length or width, shows an average deviation of +13 % across all 18 vehicles in Fig. 11.

One possible reason for the positive deviations is the methodology itself, the aim of which is to provide a generally valid approach for all vehicles by using the previously presented dimensions such as L209-2, H297-2 and W201, which are determined identically for all vehicles. Individual solutions in the trunk design, which lead to larger deviations, are therefore not taken into account. Although the method differentiates between different spring variants in the modeling of the trunk and thus enables an objective basis for comparison, individual solutions in the area of the chassis can also lead to deviations. The latter is evident in the BMW iX. The manufacturer chooses an air suspension on the rear axle, which is wider than comparable spring-damper elements [58,59]. In the simulation, this results in a smaller trunk width. The real BMW iX has the trunk floor placed higher up, avoiding the problem. An example where large differences in the individual parameters for trunk modeling result in a large deviation in the trunk volume is the Nio ET7. Its simulated trunk length exceeds the real measure, which can be explained by the fact that Nio is focusing on large legroom to maximize comfort in the second seat row, which plays an important role in a luxury sedan like the Nio ET7 [34].

In contrast to the positive deviations, the simulated trunk volume of the Tesla Model 3 is 19 % smaller than the real one. One reason for this difference is the combination of a comparatively small modeled trunk length and height in relation to other sedans' large real trunk volume [60].

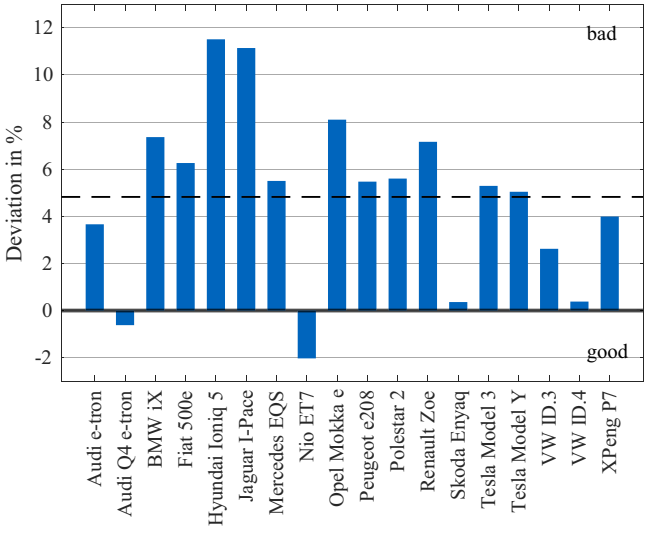

Fig. 10. Deviations in L50-2 for all 18 vehicles.

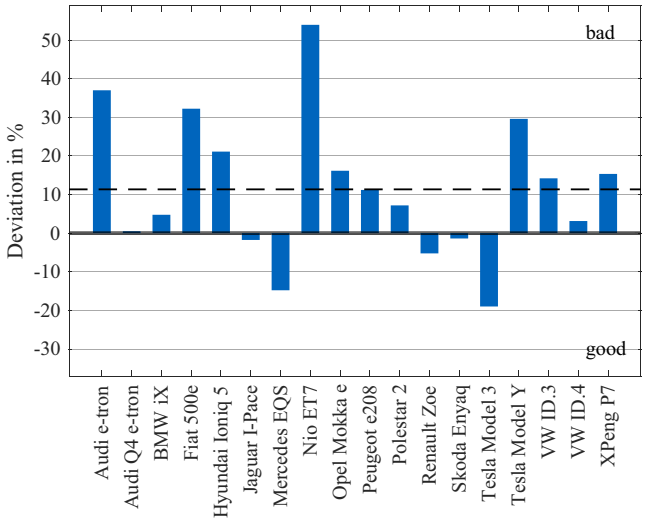

Fig. 11. Deviations in the trunk volume for all 18 vehicles.

4. Vehicle dynamics simulation

To evaluate the driving dynamics properties of electric vehicles in scientific benchmarks, this study includes a simulation of the vehicle's driving dynamics. As common in the state-of-the-art, this is divided into longitudinal and lateral dynamics. The associated methodologies are presented in the following sections. In addition, a vehicle-specific simulation of the charging time in the charging stroke from 10 to 80 % is included.

4.1. Longitudinal vehicle simulation

The longitudinal simulation is based on [61] with adapted functions and input parameters. The simulation uses the previously determined values for the scaled electric machine and the calculated vehicle mass. Based on the data, missing inputs (e. g. the moment of inertia) are determined. The longitudinal simulation is divided into acceleration, consumption, and range.

4.1.1. Acceleration simulation

The acceleration simulation determines the acceleration time from $0-100$ km/h. The first step determines the achievable wheel torque from standstill to maximum motor speed. In the second step, the acceleration and resulting velocity are calculated in an iterative approach. In each iteration, the resistance force is determined and compared to the propelling force of the powertrain. The iterations' resulting acceleration and velocity are stored in a third step. These three steps are repeated with the updated velocity. During the calculation, the traction limits depending on vehicle parameters are considered to prevent excess of these limits.

4.1.2. Consumption and range simulation

The consumption simulation allows us to evaluate the efficiencies by determining the consumption in a desired driving cycle. The preselected driving cycle for the consumption calculation is the WLTP cycle. We use the resulting reference model as the input after all the previous steps in the reference model development, including the vehicle mass. As the modeled traction battery influences the vehicle mass, the mass differs from the actual vehicle. This leads to divergent consumption results compared to the original model.

The driving resistance at every time step of the driving cycle is determined in the first step. This includes air, rolling, road gradient, and acceleration resistance. Summed up, these build the base of the consumption simulation. With the relevant vehicle parameters, the required

Table 1
Constant reference efficiencies for the consumption simulation.

Component	Efficiency	Reference
Battery	96.27 %	[63]
Power Electronics	97.48 %	[63]
Transmission	95.64 %	[62]

torque and wheel speed are transformed into the power at the wheels. We separate between front-wheel drive (FWD), rear-wheel drive (RWD), and all-wheel drive (AWD). In the case of one driven axle, in FWD and RWD, the required power of the wheels is directly converted into the mechanical power at the motor applying transmission gear ratios and efficiencies [62]. With the electric machine's efficiency map and the current torque and motor speed the efficiency is determined to compute the electrical power required at the motor. Considering the battery and power electronics' efficiencies [63], the battery's power is calculated. The used battery and power electronics efficiency represent the average of all analysed technologies in [63]. For the transmission efficiency we chose the single-speed transmission, as this is the only configuration in our simulated vehicles. The reference efficiencies are displayed in Table 1. The electric machine's efficiency is determined with three different individually scaled efficiency maps for the machine types PMSM, SSM, and IM [45].

Since the overall efficiency during braking phases is lower than during propulsion, a new and different approach has been developed for regenerative braking [64]. Based on this approach, we tested two vehicles from our institute. They represent state-of-the-art BEV from the year 2020. With several different test scenarios, including only regenerative braking, brake blending, and acceleration, the results of both vehicles were transferred into a regression model. This regression uses the power at the wheels as input and calculates the overall efficiency for the time step. This enables the direct calculation of the power being charged back into the battery while braking based on the power at the wheels. Before determining the energy consumption, the auxiliaries are considered using a constant value determined from the aforementioned two state-of-the-art BEV. In the next step, the energy consumption in the driving cycle is computed with the battery power at every time step. The consumption is calculated with the cycle's total driven distance. The last step includes the range calculation for the tested driving cycle.

For AWD vehicles, the most energy-efficient torque split between the front and rear axle is determined. For this purpose, the torque split is divided into 1 % steps, and the theoretically required power for every possible torque split is calculated. The configuration with the least required electrical power for each time step is chosen. This is done by carrying out the previously presented steps in the acceleration process for every torque split option. The result is the operating point with the lowest resulting electrical power while providing the required torque at the wheels. The regenerative braking process equals the one-axle-driven vehicle option.

In addition to the consumption calculation, we evaluate the efficiency of a vehicle based on its range. As already mentioned in Section 2.2.3, we use the ADAC-Ecotest cycle instead of the WLTP cycle to determine the range. A further reason for the Ecotest range evaluation is the test procedure performed by the independent test organization ADAC. The Ecotest consumption is determined using the procedure equivalent to the WLTP consumption. We use each vehicle's simulated battery capacity to estimate the vehicle's range.

4.1.3. Results of the longitudinal simulation

The results for the acceleration time from 0 – 100 km /h, illustrated in Fig. 12, show an average deviation of −7 % below the real vehicles. A negative deviation indicates that the simulated acceleration time is lower than the real acceleration time. In other words, the real vehicle accelerates worse than the reference vehicle, which is why a negative deviation is evaluated as negative in the subsequent vehicle evaluation, while a positive deviation is assessed as positive.

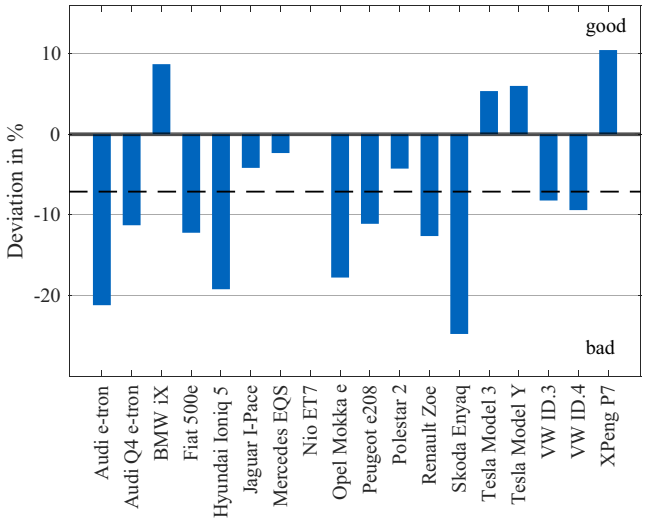

Fig. 12. Deviations in 0-100 km/h acceleration time for all 18 simulated vehicles.

The largest positive deviation compared to the real vehicle is found in the vehicles XPeng P7 (+10 %) and BMW iX (+9 %). Both corresponding real vehicles have significantly higher electric machine powers and lower masses, which leads to lower acceleration times in the real vehicles. One possible reason is that XPeng and BMW are among the latest vehicles in the benchmarking environment with sales launch in 2020/2021, so the corresponding state-of-the-art technology was comparatively well applied in both vehicles.

Conversely, a conservative configuration of the motor map and control systems can be assumed for the oldest BEV in the benchmarking: As a real vehicle, the Audi e-tron misses the simulation value. However, the real vehicle's motor output is even higher than one of the reference model with a comparable mass. With a deviation of −21 % compared to the real vehicle, the Audi e-tron is one of the vehicles with the greatest negative deviation together with the Skoda Enyaq (– 25 %) and Hyundai Ioniq 5 (– 19 %). Possible reasons for the below-average result of the acceleration simulation for the Audi are the comparatively early SOP of the vehicle and Audi's lack of experience in designing BEVs since the e-tron model was the company's first BEV.

In contrast, Skoda Enyaq and Hyundai Ioniq 5 have power-restricted motors in the drivetrain variants analyzed: According to the motor code, the Skoda has the identical electric motor in the model variant *iV50* as the higher positioned variant *iV80* (150 kW) [65]. However, only 109 kW is available in the iV50 variant. In the Hyundai, the front and rear electric machines have almost identical rotor diameters [34], but considerably less power is available in the front electric motor. The design strategy of power-restricted motors was presumably chosen by the two manufacturers in order to be able to provide cheaper entry-level variants and higher-positioned and more powerful model variants with the same electric motor in a cost-neutral way. In the context of the acceleration simulation, however, this means that the electrical machines fall below their technical capabilities in both the Skoda and the Hyundai. This explains the higher power specifications in the simulation and, thus, the significantly shorter acceleration times compared to the real vehicles.

Finally, all FWD vehicles analyzed in the simulation significantly undercut the real acceleration values: This applies equally to the Fiat 500e (– 12 %), the Opel Mokka e (– 18 %), the Renault Zoe (– 13 %) and the Peugeot e208 (– 11 %). This is due to the significantly higher motor power outputs in the simulation. One possible reason for the big difference in performance is that manufacturers limit the motor torque for starting from standstill to avoid excessive wheel spin at full accel-

eration. This explanation is reasonable because the four vehicles mentioned were designed rather as city vehicles for which a high level of driving safety is more important than maximum longitudinal dynamic performance.

The consumption simulation shows an average deviation of −2 % from the real WLTP-results. All deviations of the investigated vehicles are plotted in Fig. 13.

Compared to the results in [61] with an average deviation of − 10 %, we improved the simulation accuracy through the presented changes. We identified two main reasons for consumption deviations. Firstly, the vehicle mass, greatly influenced by the battery concept of the simulated reference model, affects the longitudinal simulation. Secondly, an older model year correlates with lower deviations. The efficiencies in the simulation represent state-of-the-art values from 2021 to 2022 [62,63]. From the analyzed vehicles, eight were released before 2021, nine are from 2021, and one is from 2022. Evaluation of the deviation confirms the trend of older vehicles having larger negative deviations than vehicles from 2021 and 2022. The Audi e-tron, released in 2019, was Audi's first series production BEV. The simulated consumption with 19.5 kWh/100km is −15 % under the official WLTP-result of 23.00 kWh /100km. This trend can also be seen in the Jaguar I-Pace from 2018 with a deviation of − 15 %. An example of a more modern vehicle with a positive deviation is the Fiat 500e from 2021. The simulated consumption is +11 % higher than the real one. The comparatively best vehicle is the Tesla Model 3 from 2020, with a deviation of +17 %. The Model 3 performs comparatively well in independent tests regarding efficiency, achieving 5 Green stars and a weighted overall index of 9.8 in the Green NCAP [66]. Additionally, the low mass is beneficial in the simulation. The Fiat 500e is the test's lightest vehicle.

The Ecotest range of the real vehicle is calculated based on the battery net capacity and the Ecotest consumption. Due to [43], both values include charging losses, which are eliminated when calculating the range. For vehicles without an ADAC-Ecotest and therefore no available range or capacity data, we used data of over 60 tested vehicles by the ADAC [32] and estimated the necessary values applying linear regression. The deviations between simulated and real range are shown in Fig. 14.

Results of the range calculation show an average deviation of -3 %. Although the average deviation is low, there are deviations up to 30 % in both directions. The variations derive mainly from differences between simulated and real battery capacities and consumptions. One example of a significant deviation is the Audi e-tron. The divergence of around − 15 % in the consumption and a large battery capacity in the reference model show the vehicle's potential. The cell dimensions installed in the

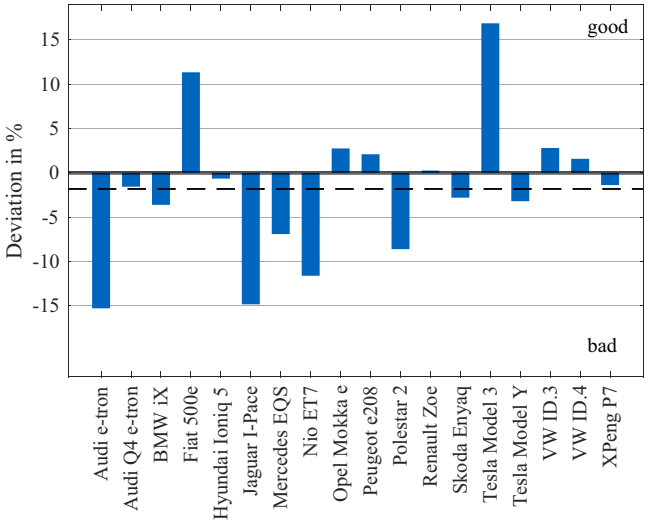

Fig. 13. Deviations in consumption for all 18 simulated vehicles.

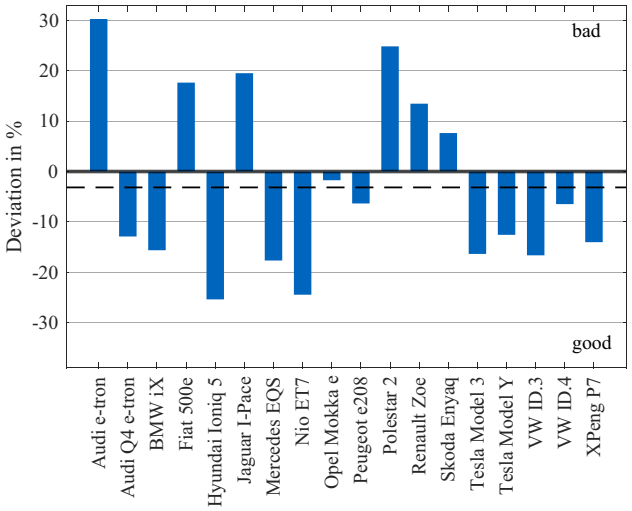

Fig. 14. Deviations in range for all 18 simulated vehicles.

digital reference model are distinct from the ones installed in the real vehicle. This leads to a distribution concept with twice the number of cells in the second level of the reference model. Besides, the net-to-gross factor of the real Audi e-tron is slightly lower than the computed mean value, yielding an additional growth of the capacity of about 4 kWh. Variations in consumption and capacity result in a relative range deviation of +30 %, indicating that our reference model achieves a significantly higher range than the real vehicle. Audi confirmed the potential in these two factors with the e-tron model improvement Audi Q8 e-tron. It has a 20 kWh higher battery capacity and a lower consumption [67]. This consequently leads to a higher range. Another example of a large positive deviation is the Polestar 2. Although detailed battery data and package factors are not available for this model, the real package factors are assumed to be significantly higher than the computed averaged ones. Hence, the cell dimensions of the digital reference model are precisely larger than the real dimensions, leading to a higher simulated battery capacity. Polestar has, analogously to Audi, already presented a model improvement, which is characterized not only by an increase in capacity but also by a reduction in consumption [68].

Considering vehicles with a large negative deviation, similar reasons can be found for their variance. Starting with the Mercedes EQS, the simulation shows a much lower available L_{batt} than the real vehicle. One reason is the scaling of the rear machine. Because of the large torque the real electric machine provides, a higher scaling factor is computed, yielding a larger extent of the machine in a horizontal direction. Due to the smaller L_{batt}, the cell dimensions in the simulated vehicle are smaller than the real ones. The Hyundai Ioniq 5 and Nio ET7 also show larger deviations in L_{batt} and, consequently, a comparable difference in the cell dimensions. Additionally, all three vehicles are characterized by a high volumetric energy density. For example, while the simulation uses a mean energy density of 521.2 WhL^{-1} for pouch cells, the cells installed in the Hyundai Ioniq 5 have a volumetric energy density of 644.9 Whl^{-1}.

4.2. Lateral dynamics simulation

The analysis of lateral dynamics follows the overall objective of the framework: While lateral dynamic evaluations in the automotive press such as AMS also include subjective evaluation components, this framework is intended to enable a purely objective, data-based evaluation of the lateral dynamics potential for different vehicles. To implement this objective, we developed a regression-based approach that uses publicly available data and evaluates the lateral dynamics based on the driving maneuver of the 18m slalom. The regressively determined slalom speeds can be compared with real measured slalom speeds, which

enables an assessment of how above or below average a vehicle was designed in the area of lateral dynamics within the scope of its technical possibilities.

4.2.1. Model Choice and Data Basis

We chose the mathematical method of multiple linear regression for the regression-based lateral dynamics analysis. For this purpose, it was first necessary to build up a suitable data set based on publicly available data and to define a parameter to evaluate lateral dynamics. Both requirements were predetermined by the measured driving maneuvers of the automotive press since it was the only available source providing sufficient data at the time of data set creation.

To assess lateral dynamics, we selected the 18m slalom as our reference: This driving maneuver is used to evaluate the general vehicle handling [69]. The test setup for the maneuver is shown in Fig. 15, whereby the test driver has to drive around the 10 cones as quickly as possible. The average speed is measured using a light barrier-based time recording system.

To ensure comparability to the 18m slalom measurements, we used *AMS* as the sole data source: The magazine offers an adequately large number of BEV measurements with sufficient comparability of the test conditions: Although *AMS* tests vehicles all year round and accordingly at different asphalt and air temperatures, the test drives are always carried out in dry conditions on the same test track and on preheated summer tires [70].

The data set created for the regression comprises a total of 67 BEV vehicles of different body shapes (hatchback: 20, saloon: 13, Sports Utility Vehicle (SUV): 32, vans: 2 vehicles) and different vehicle classes. Accordingly, the data set represents a sufficiently general vehicle cohort regarding body shape and vehicle class. It can, thus, be regarded as a reference for the current state-of-the-art. To ensure comparability, only the measured values with activated Electronic Stability Program (ESP) were recorded, as this cannot be deactivated in all vehicles.

4.2.2. Structure of the regression analysis

In the data set created, the following independent variables were found to be statistically significant concerning the test speed in the 18m slalom: Firstly, the ratio of averaged track width of the front and rear axle and vehicle height as parameters for the center of gravity height and the magnitude of dynamic wheel loads when cornering [71]. Secondly, the averaged tire sidewall height as a measure of tire cornering stiffness as well as the maximum lateral forces that can be applied when cornering [72]. Thirdly, the vehicle mass as a further measure of the level of dynamic wheel loads when cornering.

The corresponding regression formula has an adjusted coefficient of determination of 64 % and is used to simulate the slalom speed of the reference vehicle. For this purpose, the track width, the height of the real vehicle, the calculated vehicle mass and, to ensure comparability of the simulated slalom value with the *AMS* measured value of the real vehicle, the *AMS* test tire dimensions are used.

4.2.3. Results of the lateral dynamics simulation

The deviations between simulated and real slalom speed, which are illustrated in Fig. 16, show an average deviation of +0.74 % for the 18 benchmarked vehicles.

This numerically low deviation shows that the generality of the vehicles can be mapped with high accuracy using the selected approach, i.

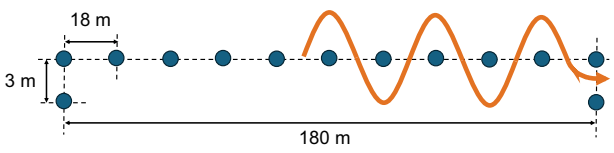

Fig. 15. 18m-slalom driving maneuver [70].

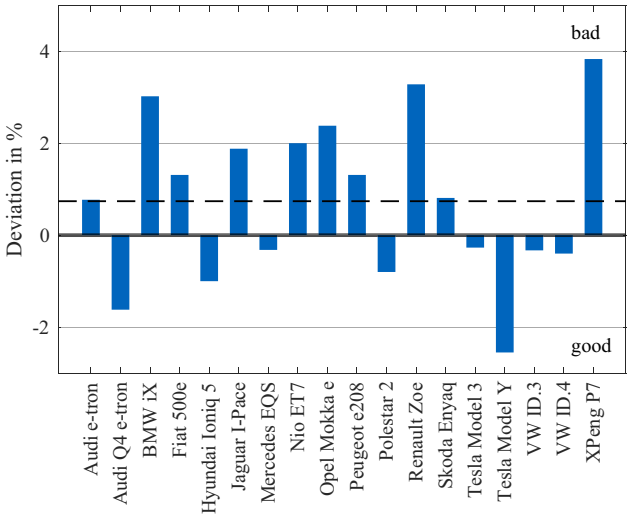

Fig. 16. Deviations in slalom velocity for all 18 vehicles.

e. the initial objective of providing an objective evaluation approach for different vehicles is fulfilled.

Among the analyzed vehicles, the Tesla Model Y (-3 %) and Audi Q4 e-tron (-2 %) have the largest negative deviation of the simulation value from the *AMS* results. XPeng P7 (+4 %), Renault Zoe, and BMW iX (both +3 %) show the greatest positive deviation compared to the ones by *AMS*.

The below-average performance of the XPeng P7 in the *AMS* slalom test (+4 %) contradicts expectations: As a sedan with a low center of gravity and a multi-link rear axle, the vehicle has favorable prerequisites for a high slalom speed. However, based on the test results, a conservative setup of the ESP can be assumed: *AMS* states in its test that the P7 is slowed down early by the ESP during road tests [73]. On the one hand, a possible reason for this ESP control strategy, which suggests a lack of fine-tuning, is the fact that XPeng, as a respectively newly founded car manufacturer (2014), has less expertise in tuning chassis than established car manufacturers. On the other hand, in view of the comparatively low selling price, it can be assumed that less money was invested in fine-tuning of chassis and suspension: This process is carried out by dedicated test engineers [69], which requires a considerable amount of time and costs.

The below-average performance of the BMW iX can be explained by the chassis setup of the xDrive50 motor variant: As *AMS* states in the test, the chassis setup is comfort-oriented and shows a tendency to roll in road tests [74]. This chassis setup was presumably chosen to maximize ride comfort, which is an important feature in the upper mid-range class. However, the low spring rates required in this design strategy in conjunction with the high body of an SUV result in higher dynamic wheel load differences when cornering and, therefore, higher slip angle requirements on the axles. This results in lower speeds in the road test.

The same applies to the Renault Zoe (+4 %): *AMS'* test reveals a comfort-oriented chassis setup with a tendency to roll [75], suggesting that low spring rates were used. The effect on the slalom speed in combination with the relatively high body for a hatchback (Renault Zoe: 1562 mm, Peugeot e208: 1430 mm) is comparable to the BMW iX. Another reason for the below-average performance compared to the simulation is the fact that the Renault has a twist-beam rear axle, which has a low lateral stiffness [69]. Therefore, less lateral force compared to a multi-link rear axle can be transmitted. The lower achievable lateral acceleration results in lower speeds in the road test. The negative influence of the twist beam rear axle also appears on the other vehicles equipped with this axle design: For Fiat 500e, Peugeot e208 (both +1 %) and Opel Mokka e (+2 %), the simulated values are all higher than the *AMS* results of the real vehicles. These findings, therefore, show that a

multi-link rear axle allows higher cornering speeds due to the higher lateral stiffness.

In contrast, for the vehicle with the largest negative deviation, the Tesla Model Y, the opposite reasoning applies as for the BMW iX and Renault Zoe: The Tesla Model Y was found to have a firm suspension setup in the *AMS* test [76]. This fact indicates that Tesla has set the spring rates to such a high level that, despite the high SUV body, comparatively low wheel load differences occur when cornering. This allows for higher cornering speeds. The AWD, which enables better vehicle handling characteristics compared to two-wheel drive (2WD) vehicles due to additional degrees of freedom in vehicle dynamics control [77], is another factor that has a positive effect on the slalom speed of the real vehicle.

Finally, the Audi Q4 e-tron, which performs significantly better compared to the other MEB-based SUV Skoda Enyaq and VW ID.4 (-2 %), can also be assumed to have a firmer chassis setup: In contrast to the Skoda Enyaq and VW ID.4 with RWD, the Audi Q4 e-tron has AWD and significantly higher engine power (+80 kW). Therefore, a firmer suspension setup adapted to this can be expected. Another factor for better performance in the slalom test is that, as with the Tesla Model Y, the AWD of the Q4 e-tron allows for longitudinal torque control.

4.3. Simulation of the charging time

This section describes the charging time. Analogously to the previous sections, an overview of the simulation is given, and the results are shown afterward.

4.3.1. Charging time simulation

As Section 2.2.3 mentions, the tool utilizes generic charging curves to simulate the charging time. For this purpose, four generic and standardized curves were generated based on real charging curves. To establish these generic curves, the real charging curves of the 18 evaluated vehicles were concentrated into clusters based on their qualitative distribution. Three main clusters were identified, each represented by one generic charging curve. Additionally, a fourth cluster was implemented to avoid a major gap between two clusters and thus the favoring/disfavoring of certain vehicles.

To select a certain curve, a charging factor is calculated by dividing the mean charging power inside the fast charging area and the maximal charging power. Both values, mean and maximal charging power, and the real fast charging time are provided by [33] to provide suitable data for an objective comparison. Additionally, the real net capacity is used. The simulation of the capacity may lead to a high variance. For example, the simulated capacity of the Audi e-tron is 17 % higher than the real one. Therefore, more energy is necessary to charge the battery up to 80 %-SOC, which leads to a higher charging time. Using the real net capacity prevents double evaluation of the simulated capacity and ensures comparability with the real charging time.

The charging factor determines the charging curve whose charging factor is closest to the real one. Given the real maximal charging power, the selected charging curve is scaled.

The simulation is based on the approach provided by Cao et al. [78], who calculated the charged energy using the time integral over the charging power. Our simulation estimates the charging time using Equation 2.

$$\frac{80\,\%\cdot E_{batt,real} - 10\,\%\cdot E_{batt,real}}{P_{charg,mean}\cdot\eta_{charg}}\cdot 60\,\text{min} \tag{2}$$

Instead of the integral, the average charging power $P_{charg,mean}$ is used. This mean power is calculated from the scaled generic charging curve. As coulombic efficiency η_{charg}, a value of 95 % is chosen [79].

4.3.2. Results of the charging time simulation

The most comparable between the four generic profiles representing charging factors of 0.64, 0.73, 0.79, and 0.89, respectively, is applied in the simulation. Fig. 17 shows the individual deviations for all vehicles. Applying the four charging profiles to all vehicles results in an average deviation of +0.67 %.

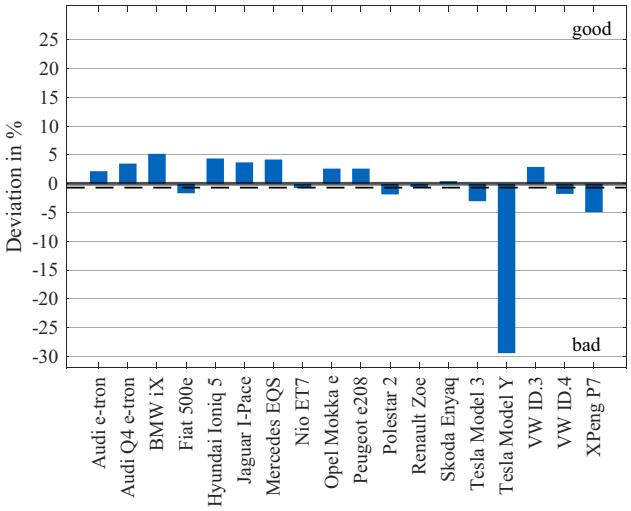

Fig. 17. Deviations in charging time for all 18 simulated vehicles.

The Tesla Model Y shows a deviation of almost -30 % due to the simulated average charging power. Using the scaled charging curve (with a charging factor of 0.64) yields an average simulated charging power of 162 kW based on the maximum charging power of the Tesla Model Y of 250 kW available only at the Tesla Superchargers [80,81]. The computed average charging power is significantly above the real average power of 108 kW. The maximum charging power of the Tesla Model Y can only be maintained for a short time at the beginning of the charging process and then drops quickly [82]. Accordingly, the real charging curve of the Tesla Model Y results in a charging factor of 0.43. This explains the large differences between simulated and real charging power. Further development of the Tesla Model Y has already yielded an increased mean charging power up to 124 kW [83].

The BMW iX and the Mercedes Benz EQS show a positive deviation of up to 5 %. A charging curve with a lower charging factor than the real one is selected for both vehicles. For example, the real charging factor of the BMW iX is 0.76. Therefore, the simulated curve with a factor of 0.73 is selected. This results in a lower average charging power of the digital reference model and, consequently, a higher simulated charging time. The same behavior can be observed when looking at the Hyundai Ioniq 5. However, with a deviation of the charging time of just under one minute, the method shows feasible results for an exemplary vehicle with an 800 V-architecture [84].

The simulation behaves oppositely for the Tesla Model 3 and Polestar 2. A simulated charging curve with a higher charging factor is used for both vehicles. This leads to a higher average charging power of 110 kW for the Tesla Model 3 (compared to 105 kW for the real vehicle) and, therefore, to a lower simulated charging time. However, the charging efficiency of the Tesla 3 has a mitigating influence on the deviation in charging time, as the real vehicle can achieve an efficiency of up to 99 % when charging at a Tesla Supercharger [85].

5. Electric vehicle engineering quality evaluation

To evaluate the engineering quality of an electric vehicle concept, the here presented approach compares the real vehicle concept with its reference model. By this procedure, the initial evaluation of a vehicle is solely based on measurable evaluation criteria and their realization of the vehicle concept compared with the state-of-the-art, which the reference model represents.

In this section, the whole evaluation process within the tool is described and discussed using an example vehicle. For this purpose, the Hyundai Ioniq 5 was selected because it achieves an average score in the final ranking with best-in-ranking and worst-in-ranking individual results. The section concludes with an exemplary benchmark of 18 existing electric vehicle concepts and a discussion of the results.

The evaluation process can be separated into four steps, which are represented by the following Sections. First, the single-vehicle attributes are evaluated based on their deviation from the reference model. In the second step, the individual scores for the vehicle attributes are calculated. Then, the combined scores are derived from the individual scores. Finally, vehicle concepts are compared, and a benchmark is created.

5.1. Evaluation of vehicle characteristics

Electric vehicle concepts can be evaluated based on various criteria, which are subjectively determinable or immeasurable. Only the previously presented objectively measurable evaluation criteria were chosen for the scope of this engineering quality evaluation. They can be separated into performance-related and comfort-related criteria. To evaluate the performance of a vehicle concept we use the acceleration time from $0-100\,\mathrm{km/h}$, the consumption according to the WLTP [42], the electric range according to the ADAC Eco-Test [43], the charging time and the slalom velocity as described in Section 4.2. For the assessment of comfort, we apply four evaluation criteria. H61-1 and H61-2 describe the available head space in the first and second row, respectively. L50-2 defines the leg space of the rear passengers. The fourth comfort criterion is the trunk volume.

The criteria selection is based on the importance of the connected customer values and publicly available car reviews. The selection should be seen as exemplary and not as an all-embracing selection of criteria to completely evaluate a BEV in all vehicle characteristics. Based on the desired benchmark different criteria can be chosen. The electric range, consumption, and charging time are still important purchase criteria [86,87]. These criteria directly relate to the extent of how well a BEV is engineered in its electric-specific characteristics [9,88]. To incorporate driving dynamics, the acceleration time was chosen for longitudinal dynamics and the slalom velocity for lateral dynamics accordingly [69,89]. Both criteria allow an initial evaluation of the realized driving dynamics by the engineers. Headroom and legroom influence the perceived personal space of the driver and thus significantly the experienced seat comfort [90]. They describe how well the interior package was designed by the engineers.

For all of the nine evaluation criteria the deviation Δx of the simulated value of the reference model x_{sim} from the realized value in the real vehicle concept x_{real} is calculated by

$$\Delta x = \frac{x_{\mathrm{sim}} - x_{\mathrm{real}}}{x_{\mathrm{real}}} \cdot 100\%. \tag{3}$$

The deviations are used as percentages. A positive deviation describes a lower realized value in the real vehicle concept than the reference model. A negative deviation relates to a higher realized value in the real vehicle concept compared to the reference model.

For the example vehicle, the Hyundai Ioniq 5, the deviations in Fig. 18 were calculated based on its simulated reference model. The results of the example vehicle encompass all possible scenarios: superior, similar, or inferior realized values compared to the reference model. For example, the deviation in the electric range of $-25\,\%$ indicates a significant improvement in the real vehicle concept compared to the state-of-the-art. The consumption deviation is $-0.65\,\%$, implying a consumption level comparable to the state-of-the-art. Conversely, the deviations of the comfort criteria are all positive, indicating that the real vehicle concept is behind the state-of-the-art in terms of comfort. The deviation of the trunk volume is $+21\,\%$. However, the deviations alone are insufficient to evaluate the vehicle characteristics, so individual scores must be introduced.

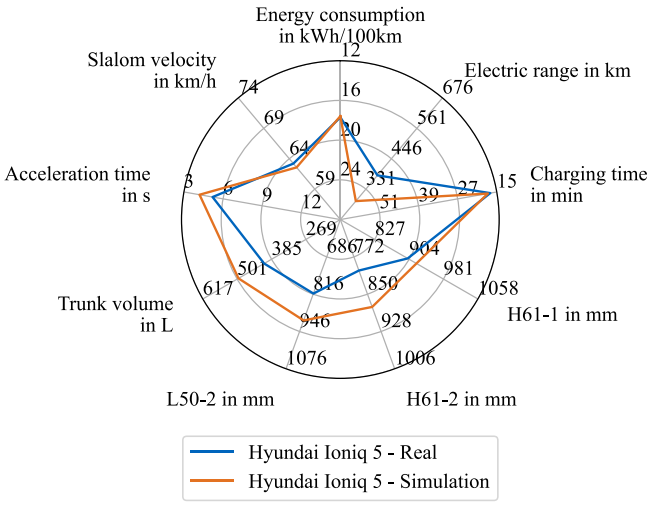

Fig. 18. Results of the vehicle individual evaluation between the real vehicle and the reference model exemplary shown on the Hyundai Ioniq 5.

5.2. Calculation of individual scores

A comparison to other vehicles is necessary to evaluate and rate an electric vehicle concept. The deviations from their reference models must also be calculated for all other vehicles in the benchmark. By using the deviation from the state-of-the-art represented by the reference model and not the absolute values of the evaluation criteria, vehicles from different vehicle classes can be compared without favoring high-priced vehicles with more expensive technologies. Based on the entire deviation data from all vehicles in a benchmark, individual scores for each evaluation criterion for every vehicle are calculated.

Since it depends on the evaluation criteria, if a positive or negative deviation is evaluated as good, the sign of the deviation must be inverted for some criteria. This adaption of the deviations leads to higher deviations, referring to better realizations of the vehicle characteristics in the real vehicle concept. But this does not imply that all deviations must be positive. Based on these adapted deviations, the individual scores of the vehicle characteristics can be calculated. Fig. 19 illustrates the calculation procedure.

The scoring scale reaches from 0 to 100 with 100 as the best score. The maximal adapted deviation $\max\Delta x$ and minimal adapted deviation $\min\Delta x$ of all vehicles in the benchmark are extracted for every evaluation criterion. These values correspond to scores $S(\max\Delta x)$ of 100 points and $S(\min\Delta x)$ of 0 points, respectively. The score $S(\Delta x_{\mathrm{veh.X}})$ for a specific deviation is then calculated by linear interpolation using the following equation

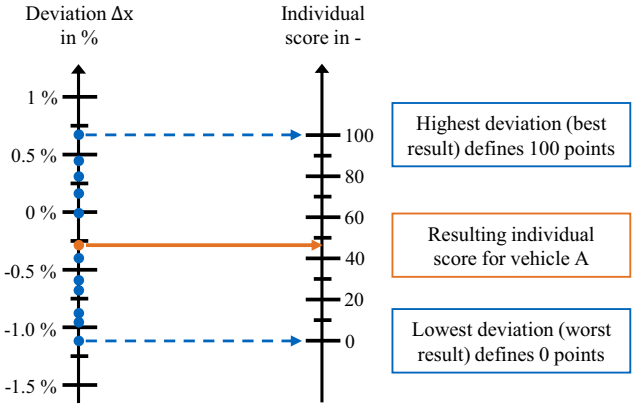

Fig. 19. Calculation procedure of the individual scores.

$$S(\Delta x_{\text{veh.X}}) = S(\min\Delta x) + (\Delta x_{\text{veh.X}} - \min\Delta x) \cdot \frac{S(\max\Delta x) - S(\min\Delta x)}{\max\Delta x - \min\Delta x}. \quad (4)$$

This calculation scheme shows that the scores of the evaluated vehicle concept depend on how the other vehicles in the benchmark perform in comparison. For example, if more vehicles in the benchmark have a better vehicle concept than the state-of-the-art, the median is set to a higher standard. Therefore, vehicles are penalized more for underperforming the state-of-the-art defined by their reference model. This characteristic of the evaluation scheme is also evident in the individual scores of the Hyundai Ioniq 5, which are shown in Fig. 20. The highest negative deviation in the range of the real vehicle compared to its simulation reference presented in Section 5.1 results in a maximum score of 100. Thus, the Hyundai Ioniq 5 is the best vehicle in the electric range within the benchmark in this study. This is an example of a high deviation resulting in a score at the high or low end. A contrary example of a high deviation that does not directly lead to a high score is the trunk volume. The example vehicle has a high deviation of +21 % but scores a mediocre 45 points in the evaluation criterion. This is a good example that not the actual values or the absolute deviations decide the rating but the deviation from the state-of-the-art compared to the other vehicles in the benchmark. The deviation of the consumption of the example vehicle is near 0 %, resulting in an individual score of 45.5 and not 50. This illustrates that the scale depends on the entire benchmark of vehicles and that 50 points do not directly correlate to the state-of-the-art. Fig. 20 also shows two other vehicles, vehicle B from the upper end of the final benchmark and vehicle C from the lower end. The edges of the area of vehicle B show results of 46 points and higher, whereas the edges of vehicle C only surpass the 50 points in two evaluation criteria. Whereas the edges present the individual results in their respective criteria, the area is a clear indicator of whether a vehicle is an overall highly ranked or rather lower ranked vehicle. Fig. 20 not only presents rather lower specific results for vehicle C, but the area is the smallest compared to the other illustrated vehicles. The figure shows that the Hyundai Ioniq 5 ranks between the two vehicles. The overall performance significantly influences the final benchmark result, combining the individual scores.

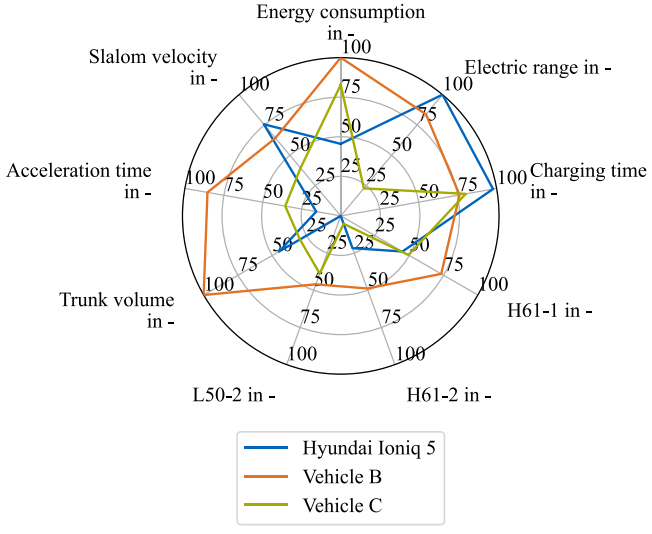

Fig. 20. Results of multiple vehicle evaluation with the transferred characteristics into point scores exemplary shown on the Hyundai Ioniq 5 and two other vehicles within this study.

5.3. Derivation of combined scores

The individual scores calculated according to Section 5.2 are the most basic evaluation level. They allow a distinctive benchmark in each of the evaluation criteria. A combination of the individual scores is beneficial for a more abstract and high-level evaluation of an electric vehicle concept. Combined scores allow the clustering of vehicle characteristics and emphasis on specific areas of the benchmark. Here, a weighted sum of individual scores as a combined score is proposed.

5.3.1. Definition of the weight factors

To consider specific customer preferences in the benchmark, we conducted a survey to determine the weighting factors. Other options to define the weighting factors could be using expert rankings, individual weighting based on the benchmark goal, and homogenous weighting of all criteria. For the results of this study, a survey with 79 participants with academic or industrial backgrounds in automotive engineering was conducted. The average age of the respondents is 28, and the gender distribution is 92 % male and 8 % female. Due to the inhomogeneous gender distribution the representativeness is limited. The respondents were asked to sort the aforementioned evaluation criteria by descending importance. The H61-1 and H61-2 measure were combined to head space and the L50-2 measure was paraphrased as leg space. This does not impede the combination of these individual scores as shown in Section 5.3.2. The weight factor w_x for each evaluation criterion x is therefore calculated as

$$w_x = \frac{\sum_{i=1}^{n} N_{x,i} \cdot (n + 1 - i)}{p \cdot \sum_{i=1}^{n} i} \quad (5)$$

with n as the count of evaluation criteria, p the number of survey participants and $N_{x,i}$ the sum of all votes for the criterion x with the importance rating i. Thus, the weight factor is between 0 and 1.

The survey results revealed the weight factors in Table 2 calculated as described above. The electric range, charging time, and consumption are still the most important customer-related features for the survey respondents, while leg space is rated as least important.

5.3.2. Calculation of the combined scores

Which evaluation criteria should be combined into more high-level scores is an individual decision and depends on the benchmark's scope. For the scope of this study, all evaluation criteria are combined into one Engineering score. The term Engineering score was chosen because the evaluation procedure represents a measure of how well the electric vehicle was engineered compared to the state-of-the-art.

In the first step, the individual scores of H61-1 and H61-2 are combined into one Z-direction score. This is done to ensure that for comfort criteria every axis of the coordinate system is weighted equally. Since for the X-direction, only one evaluation criterion is considered, and for coherent naming, the L50-2 score is renamed to the X-direction score. Due to these changes, the survey in Section 5.3.1 can subsequently be

Table 2
Weight factors of all evaluation criteria based on the results of the presented survey.

Evaluation criterion	Weight factor in %
acceleration time	9.5
consumption	15.5
electric range	19.7
charging time	17.7
slalom velocity	9.7
head space	10.2
leg space	6.6
trunk volume	11.0

used to calculate the weight factors for the Engineering score without explicitly asking for the SAE comfort measures.

In the second step, the Engineering score is calculated as a weighted sum of all evaluation criteria with the weight factors in Table 2.

The example vehicle, Hyundai Ioniq 5, achieves an Engineering score of 61.3. Even though the vehicle scores below 50 points in all comfort-related evaluation criteria and was worst-in-class in leg space within the benchmark in this study, high scores in evaluation criteria with high weight factors compensate for the below-average rating for comfort. Especially reaching 100 points in the electric range with the highest weight factor contributes to that. This illustrates how important a thorough definition of the weight factors is and what influence they have on the final results.

5.4. Benchmark of electric vehicle concepts

The final step of the presented evaluation process is the benchmarking of multiple vehicles based on the calculated Engineering score. Whereas a benchmark based on a single individual score allows conclusions on specific customer-related features, benchmarks based on combined scores allow a more high-level rating of vehicle concepts. Various automotive magazines also use a final score that combines all evaluation criteria to assign a final assessment to a vehicle. These scores determine the best vehicle concept in a specific category or an overall best concept.

The evaluation procedure objectively assesses electric vehicle concepts independent of their UVP. Only measurable evaluation criteria are used. By comparing the vehicle characteristics to a simulated reference model representing the state-of-the-art rather than other vehicles, the UVP is not regarded. Only in the final benchmark of multiple vehicles, these vehicles are compared against each other. Further measures are taken to ensure objectivity and comparability, including using the same sources for the real vehicle data and the same database to represent the state-of-the-art for the simulation of all vehicles.

5.5. Exemplary benchmark

Table 3 shows the ranking based on the Engineering score. The first five places in the ranking are the Tesla Model 3, Audi Q4 e-tron, Mercedes EQS, VW ID.3 and BMW iX. With an Engineering score of 80.2, the Tesla Model 3 reaches the highest score in the benchmark, outperforming the Audi Q4 e-tron by 9.3 points. This can be explained by the overall high individual scores in all evaluation criteria. The last three places are the Jaguar I-Pace, Renault Zoe, and the Audi e-tron. The Audi e-tron reaches the lowest Engineering score of 33.9 points, which is 9.52 points less than the Renault Zoe. This can also be explained by the low individual scores in evaluation criteria with high weight factors like consumption and range. The benchmarked model of the Audi e-tron (SOP in 2019) can be considered outdated compared to the here-defined state-of-the-art.

The results show that especially purpose design vehicles like the Tesla Model 3 or the Mercedes EQS achieve, on average, higher scores compared to conversion design vehicles like the Renault Zoe or the Fiat 500e. This shows that vehicles that are designed and engineered from the start as BEV without the restrictions from a conventional powertrain can offer a higher customer value. Besides, vehicles based on the same architectural platform score similarly, such as the MEB vehicles. This emphasizes the importance of thorough engineering of the platform as it significantly influences the engineering quality. One exception is the Skoda Enyaq, which scores significantly lower than the other MEB vehicles. This is rooted in the benchmarked pre-model-improvement version from 2021, for which the whole data basis was available when creating the benchmark. The presented methodology identified the motor's low torque and the small battery capacity as optimization potential. Thus the methodology can identify the optimization potential of current vehicles or concepts and help engineers to improve the characteristics during the development process of new vehicles. Both described matters were addressed by the model improvement in 2023. Another notable result is the independence of the Engineering score results from the vehicle price. In Reference to Fig. 1, Fig. 21 plots the Engineering score over the UVP with a linear trendline. The coefficient of determination R^2 for the plotted linear trendline is 0.34 %. Based on these results, no significant dependency of the Engineering score from the UVP is derived. Thus the presented methodology purely focuses on technical engineering characteristics and not on financial topics. As mentioned in Section 1, this tool's focus is on highlighting variances from the

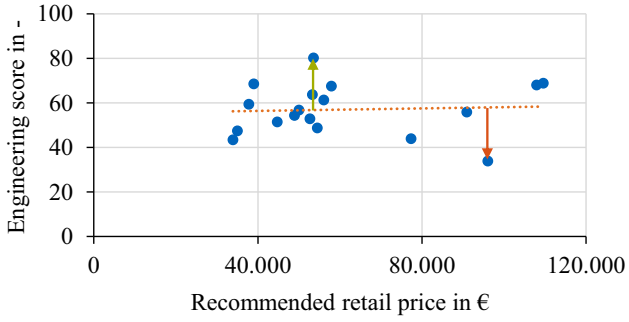

Fig. 21. Final results of the presented methodology with the 18 electric vehicle concepts within this study (blue points) with a trendline indicating independence to the UVP.

Table 3
Benchmarking results of the current state-of-the-art battery electric vehicle concepts.

Vehicle	Model	Year	Motor front (power)	Motor rear (power)	Cell chemistry	Battery capacity (net)	Engineering score
Tesla Model 3	Standard Range Plus	2021	-	PSM (239 kW)	NCA	58 kWh	80.2
Audi Q4	50 e-tron advanced quattro	2021	ASM (80 kW)	PSM (150 kW)	NMC	77 kWh	70.9
Mercedes EQS	580 4MATIC	2021	PSM (140 kW)	PSM (245 kW)	NMC	107.8 kWh	68.8
VW ID.3	Pro Performance 1st Max	2020	-	PSM (150 kW)	NMC	58 kWh	68.5
BMW iX	xDrive50	2021	FSM (190 kW)	FSM (230 kW)	NMC	105.2 kWh	68.1
VW ID.4	Pro Performance 1st	2020	-	PSM (150 kW)	NMC	77 kWh	64.3
XPeng P7	RWD Super-Long Range Zhizun	2020	-	PSM (196 kW)	NMC	75 kWh	61.3
Hyundai IONIQ 5	Project 45	2021	PSM (70 kW)	PSM (155 kW)	NMC	70 kWh	61.3
Peugeot e-208	136 GT	2020	PSM (100 kW)	-	NMC	48.1 kWh	59.4
NIO ET7	100 kWh	2022	PSM (180 kW)	ASM (300 kW)	NMC	90 kWh	57.0
Skoda Enyaq	iV50	2021	-	PSM (109 kW)	NMC	52 kWh	54.4
Tesla Model Y	Maximum Range AWD	2021	ASM (158 kW)	PSM (220 kW)	NMC	75 kWh	52.9
Opel Mokka	Electric Ultimate	2021	PSM (100 kW)	-	NMC	48.1 kWh	51.5
Polestar 2	Long Range Dual Motor	2020	PSM (150 kW)	PSM (150 kW)	NMC	75 kWh	48.8
Fiat 500e	La Prima	2020	PSM (87 kW)	-	NMC	37.3 kWh	47.4
Jaguar I-Pace	EV400 S AWD	2018	PSM (147 kW)	PSM (147 kW)	NMC	84.7 kWh	43.9
Renault Zoe	R135 Z.E. 50 Experience	2019	FSM (100 kW)	-	NMC	52 kWh	43.4
Audi e-tron	55 quattro	2019	ASM (140 kW)	ASM (160 kW)	NMC	83.6 kWh	33.9

trendline in Fig. 1 as an indicator for engineering quality. The red arrow in Fig. 21 depicts the negative deviation of the Audi e-tron from the overall trendline as an example of an expansive vehicle with a low Engineering score. As discussed before, the reasons for the low rating can be directly extracted from the simulation results. Analogously to the vehicle with the biggest positive variance to the trendline in Fig. 1, the green arrow pointing to the Tesla Model 3 illustrates the same effect in the opposite direction, presenting the overall best vehicle in our simulation result. The results from the benchmark are directly explainable and purely objective.

6. Summary and conclusions

This study provides a methodology for objective and cost-independent benchmarking analysis of the most relevant features of battery electric vehicles, with Fig. 21 proving the optimization compared to the state-of-the-art in Fig. 1. Collocating real vehicle data of 18 current BEV with state-of-the-art parameters regarding electric powertrain components, meaningful results are obtained from this work, comparing the automatically generated results to current car reviews. Applying various methods, a broad range of disciplines are considered within this analysis. The major discoveries from this study can be summarized as follows:

- **Individual vehicle evaluation through state-of-the-art reference model.** The combination of real vehicle parameters, parameters based on regressive analysis, and parameters taken from literature allows the conception of average vehicle concepts and their respective performance characteristics and comfort features. With an average electric vehicle concept based on the respective parameter set, vehicles are evaluated regarding the level of potential exploited within the vehicles' boundaries.
- **Holistic approach of identifying vehicle concept characteristics.** Based on the analysis of current electric vehicle evaluation criteria of established car reviewers, the most relevant features for customers were identified. Based on these features, different methods were implemented to identify these parameters for comparison with the real vehicle characteristics. The described methodologies are based on official standards and analytical and regression models and present meaningful and reasonable results for the respective characteristics. Considering the most relevant features, different design focuses of manufacturers were taken into account, collocating in an overall holistic final evaluation.
- **Expedient evaluation scheme weighting costumer relevant characteristics.** The most dominant deviations of specific vehicles in single features were presented and discussed in their respective sections by explanations through specific concept strategies or ideas and in reference to similar results from current reviews. The evaluation scheme shows an expedient concept of transferring the vehicle-specific results into a comparison across multiple vehicles regarding the single disciplines. Applying the results from the presented study, which carried out weighting factors for these disciplines due to the opinion of engineers in research and the automotive industry, a final score is collocated, ranking the vehicles within this study.

This methodology allows the evaluation of vehicle concepts without the need for physical prototypes. This supports engineers from the automotive industry in optimizing their concept development processes, evaluating their ideas in the early stages, and potentially deciding on better overall vehicle concepts. Also, this enables researchers to evaluate vehicle concepts cost-efficiently. With the opportunity to transfer the presented methodology to other domains (e. g. component concepts). Considering that there are many different component concepts in the electric vehicle market, superior technology concepts can be identified, and manufacturers can focus on these technologies. By adopting the weight factors according to individual focus areas, the overall focus is shifted, and results will adapt adequately, allowing for the identification of individual optimal solutions.

Data availability

We want to encourage researchers and engineers from the automotive industry to comprehend our work and to enable them to apply our methodology to their vehicle concepts, evaluate their work, and identify optimization potentials. Therefore, our methodology is provided as open source accessible via FTMGithub. Unfortunately, we cannot share the parameter data of all 18 vehicles since it is confidential, but we share the two vehicles that have been analyzed in [10,11].

CRediT authorship contribution statement

Nico Rosenberger: Conceptualization, Methodology, Investigation, Resources, Writing – original draft, Writing – review & editing, Project administration. **Moritz Fundel:** Investigation, Writing – original draft, Writing – review & editing, Visualization. **Simon Bogdan:** Investigation, Writing – original draft, Writing – review & editing, Visualization. **Lukas Köning:** Investigation, Writing – original draft, Writing – review & editing, Visualization. **Peter Kragt:** Investigation, Writing – original draft, Writing – review & editing, Visualization. **Moritz Kühberger:** Investigation, Writing – original draft, Writing – review & editing, Visualization. **Markus Lienkamp:** Resources, Supervision, Writing – review & editing, Funding acquisition.

Declaration of competing interest

The authors declare that they have no known competing financial interests or personal relationships that could have appeared to influence the work reported in this paper.

Acknowledgment

This work was funded by the German Federal Ministry for Economic Affairs and Climate Action (BMWK) within the project "ScaleUp-eDrive" under grant number 16THB0006C.

References

[1] Statista GmbH, Wer/was wird vermutlich Ihre Entscheidung bei einem Autokauf beeinflussen?, 2018, Accessed on 13.07.2023, https://de.statista.com/prognosen/856902/umfrage-in-deutschland-zu-einflussfaktoren-auf-die-entscheidung-beim-autokauf.
[2] Morning Consult, More consumers care about a Car's reviews, safety than its gas mileage., 2012,. Accessed on 13.07.2023, https://pro.morningconsult.com/articles/more-consumers-care-about-cars-reviews-safety-than-gas-mileage.
[3] auto motor und sport, E-Auto supertest mit alexander Bloch., 2023, Accessed on 13.02.2023, https://www.youtube.com/playlist?list=PLebLoMHyZWeT7L_hwPv4kZSlpL7wFZpRo.
[4] F. Momen, K. Rahman, Y. Son, Electrical propulsion system design of Chevrolet Bolt battery electric vehicle, IEEE Trans. Ind. Appl. 55 (1) (2018) 376–384, https://doi.org/10.1109/ECCE.2016.7855076.
[5] B. Sarlioglu, C.T. Morris, D. Han, S. Li, Benchmarking of electric and hybrid vehicle electric machines, power electronics, and batteries. 2015 Intl Aegean Conference on Electrical Machines & Power Electronics (ACEMP), 2015 Intl Conference on Optimization of Electrical & Electronic Equipment (OPTIM) & 2015 Intl Symposium on Advanced Electromechanical Motion Systems (ELECTROMOTION), 2015, pp. 519–526, https://doi.org/10.1109/OPTIM.2015.7426993.
[6] G. Kovachev, H. Schröttner, G. Gstrein, L. Aiello, I. Hanzu, H.M.R. Wilkening, A. Foitzik, M. Wellm, W. Sinz, C. Ellersdorfer, Analytical dissection of an automotive Li-ion pouch cell, Batteries 5 (4) (2019) 67, https://doi.org/10.3390/batteries5040067.
[7] G. Oh, D.J. Leblanc, H. Peng, Vehicle energy dataset (VED), a large-scale dataset for vehicle energy consumption research, IEEE Trans. Intell. Transp. Syst. (2020) 1–11, https://doi.org/10.1109/TITS.2020.3035596.
[8] J. Diez, Advanced vehicle testing and evaluation, final technical report encompassing project activities from October 1, 2011 to April 30, 2018. Technical Report, Intertek Testing Services, NA, Inc., Arlington Heights, IL (United States), 2018, https://doi.org/10.2172/1481912.
[9] E.A. Grunditz, T. Thiringer, Performance analysis of current bevs based on a comprehensive review of specifications, IEEE Trans. Transp. Electrificat. 2 (3) (2016) 270–289, https://doi.org/10.1109/TTE.2016.2571783.

[10] N. Wassiliadis, M. Steinsträter, M. Schreiber, P. Rosner, L. Nicoletti, F. Schmid, M. Ank, O. Teichert, L. Wildfeuer, J. Schneider, A. Koch, A. König, A. Glatz, J. Gandlgruber, T. Kröger, X. Lin, M. Lienkamp, Quantifying the state of the art of electric powertrains in battery electric vehicles: range, efficiency, and lifetime from component to system level of the Volkswagen ID.3, eTransportation 12 (2022) 100167, https://doi.org/10.1016/j.etran.2022.100167.

[11] N. Rosenberger, P. Rosner, P. Bilfinger, J. Schöberl, O. Teichert, J. Schneider, K. A. Gamra, C. Allgäuer, B. Dietermann, M. Schreiber, M. Ank, T. Kröger, A. Köhler, M. Lienkamp, Quantifying the state of the art of electric powertrains in battery electric vehicles: comprehensive analysis of the tesla model 3 on the vehicle level, World Electric Veh. J. 15 (6) (2024), https://doi.org/10.3390/wevj15060268.

[12] D. Piromalis, A. Kantaros, Digital twins in the automotive industry: the road toward physical-digital convergence, Appl. Syst. Innovat. 5 (4) (2022), https://doi.org/10.3390/asi5040065.

[13] W.A. Ali, M.P. Fanti, M. Roccotelli, L. Ranieri, A review of digital twin technology for electric and autonomous vehicles, Appl. Sci. 13 (10) (2023), https://doi.org/10.3390/app13105871.

[14] L. Kumar, S. Jain, Electric propulsion system for electric vehicular technology: a review, Renew. Sustain. Energy Rev. 29 (2014) 924–940, https://doi.org/10.1016/j.rser.2013.09.014.

[15] F. Naseri, S. Gil, C. Barbu, E. Cetkin, G. Yarimca, A. Jensen, P. Larsen, C. Gomes, Digital twin of electric vehicle battery systems: comprehensive review of the use cases, requirements, and platforms, Renew. Sustain. Energy Rev. 179 (6) (2023), https://doi.org/10.1016/j.rser.2023.113280.

[16] L. Nicoletti. Parametric modeling of battery electric vehicles in the early development phase, Technical University of Munich, Munich, 2022 phd thesis.

[17] L. Nicoletti, A. Romano, A. König, P. Köhler, M. Heinrich, M. Lienkamp, An estimation of the lightweight potential of battery electric vehicles, Energies 14 (15) (2021) 4655, https://doi.org/10.3390/en14154655.

[18] L. Nicoletti, W. Schmid, M. Lienkamp, Databased architecture modeling for battery electric vehicles. 2020 Fifteenth International Conference on Ecological Vehicles and Renewable Energies (EVER), IEEE, Monte-Carlo, Nonaco, 2020, pp. 1–9, https://doi.org/10.1109/EVER48776.2020.9242995.

[19] SAE J1100, Motor vehicle dimensions.

[20] ISO 4130, Road Vehicles - 3-dimensional reference system and fiducial marks - Definitions.

[21] A. Müller, Systematische und nutzerzentrierte Generierung des Pkw-Maßkonzepts als Grundlage des Interior-und Exteriordesign, 2010.

[22] J. Hahn, Eigenschaftsbasierte Fahrzeugkonzeption, Springer, 2017.

[23] P.K. Singh, S.C. Jain, P.K. Jain, Advanced optimal tolerance design of mechanical assemblies with interrelated dimension chains and process precision limits, Comput. Ind. 56 (2) (2005) 179–194, https://doi.org/10.1016/j.compind.2004.06.008.

[24] M. Felgenhauer, F. Schöpe, M. Bayerlein, M. Lienkamp, et al., Derivation, analysis and comparison of geometric requirements for various vehicle drivetrains using dimensional chains. Proceedings of the 21st International Conference on Engineering Design (ICED 17) Vol 4: Design Methods and Tools, 2017, pp. 189–198.Vancouver, Canada

[25] M.F. Felgenhauer. Automated Development of Modular Systems for the Vehicle Front of Passenger Cars, Technical University of Munich, 2019 phd thesis.

[26] T. Hofman, M. Steinbuch, R. van Druten, A.F. Serrarens, Design of CVT-based hybrid passenger cars, IEEE Trans. Veh. Technol. 58 (2) (2008) 572–587, https://doi.org/10.1109/TVT.2008.926217.

[27] L. Nicoletti, F. Ostermann, M. Heinrich, A. Stauber, X. Lin, M. Lienkamp, Topology analysis of electric vehicles, with a focus on the traction battery, Forschung im Ingenieurwesen (2020).

[28] B. Wang, D.L.-S. Hung, J. Zhong, K.-Y. Teh, Energy consumption analysis of different BEV powertrain topologies by design optimization, Int. J. Automot. Technol. 19 (2018) 907–914, https://doi.org/10.1007/s12239-018-0087-z.

[29] L. Nicoletti, P. Köhler, A. König, M. Heinrich, M. Lienkamp, Parametric modeling of weight and volume effects in battery electric vehicles, with focus on the gearbox, Proc. Des. Soc. 1 (2021) 2389–2398, https://doi.org/10.1017/pds.2021.500.

[30] J. Larminie, J. Lowry, Electric Vehicle Technology Explained, John Wiley & Sons, 2012.

[31] F.A. Machado, P.J. Kollmeyer, D.G. Barroso, A. Emadi, Multi-speed gearboxes for battery electric vehicles: current status and future trends, IEEE Open J. Veh. Technol. 2 (2021) 419–435, https://doi.org/10.1109/OJVT.2021.3124411.

[32] Allgemeiner Deutscher Automobil-Club e.V., Automarken & Modelle, 2023, https://www.adac.de/rund-ums-fahrzeug/autokatalog/marken-modelle.

[33] EV Database, Ev database, 2023, https://https://ev-database.org.

[34] A2MAC1, Home, 03.08.2023, https://www.a2mac1.com/.

[35] H. Bubb, R.E. Grünen, W. Remlinger, Anthropometric vehicle design, in: H. Bubb, K. Bengler, R.E. Grünen, M. Vollrath (Eds.), Automotive Ergonomics, Springer Fachmedien Wiesbaden, Wiesbaden, 2021, pp. 343–468, https://doi.org/10.1007/978-3-658-33941-8_7.

[36] T. Woehrle, Lithium-ion cell, in: R. Korthauer (Ed.), Lithium-Ion Batteries: Basics and Applications, Springer Berlin Heidelberg, Berlin, Heidelberg, 2018, pp. 101–111, https://doi.org/10.1007/978-3-662-53071-9_9.

[37] L. Nicoletti, A. Romano, A. König, F. Schockenhoff, M. Lienkamp, Parametric modeling of mass and volume effects for battery electric vehicles, with focus on the wheel components, World Electric Veh. J. 11 (4) (2020) 63, https://doi.org/10.3390/wevj11040063.

[38] C. Xu, Q. Dai, L. Gaines, M. Hu, A. Tukker, B. Steubing, Future material demand for automotive lithium-based batteries, Commun. Mater. 1 (1) (2020) 99, https://doi.org/10.1038/s43246-020-00095-x.

[39] SAE International, Sae j826: devices for use in defining and measuring vehicle seating accommodation.

[40] O. Sureiman, C.M. Mangera, F-test of overall significance in regression analysis simplified, J. Practice Cardiovascular Sci. 6 (2) (2020) 116–122, https://doi.org/10.4103/jpcs.jpcs_18_20.

[41] N.L. Leech, J.A. Gliner, G.A. Morgan, R.J. Harmon, Use and interpretation of multiple regression, J. Am. Acad. Child Adolescent Psychiatry 42 (6) (2003) 738–740, https://doi.org/10.1097/01.CHI.0000046845.56865.22.

[42] E. Comission, Commission regulation (eu) 2017/ of 1 june 2017 supplementing regulation (ec) no 715/2007 of the european parliament and of the council on type-approval of motor vehicles with respect to emissions from light passenger and commercial vehicles (euro 5 and euro 6) and on access to vehicle repair and maintenance information, amending directive 2007/46/ec of the european parliament and of the council, commission regulation (ec) no 692/2008 and commission regulation (eu) no 1230/2012 and repealing commission regulation (ec) no 692/2008. https://eur-lex.europa.eu/legal-content/EN/TXT/PDF/?uri=CELEX:32017R1151.

[43] ADAC, Ecotest bewertungskriterien ab 4/21(2021). https://www.adac.de/-/media/pdf/tet/ecotest/ftkinfo-ecotest-test-und-bewertungskriterien-ab-04_2021.pdf.

[44] A. Mahmoudi, W.L. Soong, G. Pellegrino, E. Armando, Efficiency maps of electrical machines. 2015 IEEE Energy Conversion Congress and Exposition (ECCE), IEEE, 2015, pp. 2791–2799, https://doi.org/10.1109/ECCE.2015.7310051.

[45] J. Goss, Performance analysis of electric motor technologies for an electric vehicle powertrain, Wrexham, UK, Motor Design Ltd., White Paper (2019).

[46] M. Hackmann, P3 charging index report 07/22 - comparison of the fast charging capability of various electric vehicles, 2022, https://www.p3-group.com/en/p3-charging-index-comparison-of-the-fast-charging-capability-of-various-electric-vehicles-from-a-users-perspective_07-22/.

[47] Polestar, The battery of the all-electric polestar 2, 16.08.2023, https://www.polestar.com/en-kw/polestar-2/performance/car-battery-pack/.

[48] S. Stipetic, D. Zarko, M. Popescu, Ultra-fast axial and radial scaling of synchronous permanent magnet machines, IET Electric Power Appl. 10 (7) (2016) 658–666, https://doi.org/10.1049/iet-epa.2016.0014.

[49] J. Pries, H. Hofmann, Magnetic and thermal scaling of electric machines, Int. J. Veh. Des. 61 (1-4) (2013) 219–232, https://doi.org/10.1504/IJVD.2013.050849.

[50] L. Nicoletti, S. Mirti, F. Schockenhoff, A. König, M. Lienkamp, Derivation of geometrical interdependencies between the passenger compartment and the traction battery using dimensional chains, World Electric Veh. J. 11 (2) (2020) 39, https://doi.org/10.3390/wevj11020039.

[51] SAE J1052, Motor vehicle driver and passenger head position.

[52] SAE J4002, H-point machine (hpm-ii) specifications and procedure for h-point determination - auditing vehicle seats.

[53] R.J. Mau, P.J. Venhovens, Development of a consistent continuum of the dimensional parameters of a vehicle for optimization and simulation. Proceedings of the Institution of Mechanical Engineers, Part D: Journal of Automobile Engineering, COPE, 2014, pp. 591–603.

[54] T. Gear, Renault zoe review (2021). https://www.topgear.com/car-reviews/renault/zoe/interior.

[55] A.E. Magazine, Fiat 500 - practicality, comfort and boot space(2023). https://www.autoexpress.co.uk/fiat/500/practicality.

[56] Carbuzz, 2024 bmw ix interior and cargo(2024). https://carbuzz.com/cars/bmw/ix/photos-interior.

[57] Fleetnews, Audi q4 e-tron 40 long-term test | built-in systems to maximise range, 2022, https://www.fleetnews.co.uk/cars/reviews/audi-q4-e-tron-40.

[58] B.P. Bulgaria, Bmw ix - chassis (june 2021)., 2021, https://www.press.bmwgroup.com/bulgaria/photo/detail/P90423654/BMW-iX-Chassis-June-2021.

[59] B.P. Poland, Bmw ix - chassis (june 2021)., 2021, https://www.press.bmwgroup.com/poland/photo/detail/P90423662/BMW-iX-Chassis-June-2021.

[60] U.N..W.R. L.P., 2024 tesla model 3 interior review., 2024, https://cars.usnews.com/cars-trucks/tesla/model-3/interior.

[61] A. König, L. Nicoletti, S. Kalt, K. Müller, A. Koch, M. Lienkamp, An open-source modular quasi-static longitudinal simulation for full electric vehicles. 2020 Fifteenth International Conference on Ecological Vehicles and Renewable Energies (EVER), 2020, pp. 1–9, https://doi.org/10.1109/EVER48776.2020.9242981.

[62] J. Hengst, M. Werra, F. Küçükay, Evaluation of transmission losses of various battery electric vehicles, Automot. Innovat. 5 (4) (2022) 388–399, https://doi.org/10.1007/s42154-022-00194-0.

[63] N. Sorokina, J. Estaller, A. Kersten, J. Buberger, M. Kuder, T. Thiringer, R. Eckerle, T. Weyh, Inverter and battery drive cycle efficiency comparisons of multilevel and two-level traction inverters for battery electric vehicles. 2021 IEEE International Conference on Environment and Electrical Engineering and 2021 IEEE Industrial and Commercial Power Systems Europe (EEEIC / I&CPS Europe), IEEE, 2021, pp. 1–8, https://doi.org/10.1109/EEEIC/ICPSEurope51590.2021.9584705.

[64] A.E. Grunditz, T. Thiringer, Characterizing bev powertrain energy consumption, efficiency, and range during official and drive cycles from gothenburg, sweden, IEEE Trans. Veh. Technol. 65 (6) (2016) 3964–3980, https://doi.org/10.1109/TVT.2015.2492239.

[65] Skoda, Technische daten skoda enyaq iv (2022), 2022, https://www.skoda-media.de/model_motor/genpdf/23995.

[66] Green NCAP, Green ncap assessment of the tesla model 3 208 kw electric rwd automatic, 2022, 2023, https://www.greenncap.com/assessments/tesla-model-3-2022-0099/.

[67] Car, Driver, Tested: 2024 audi q8 e-tron and q8 e-tron sportback go farther, quietly (2023). https://www.caranddriver.com/reviews/a43958587/2024-audi-q8-e-tron-q8-e-tron-sportback-drive/.

[68] Polestar 2 long range dual motor (82 kwh) (ab 07/23): Technische daten, bilder, preise | adac, 06.03.2024, https://www.adac.de/rund-ums-fahrzeug/autokatalog/marken-modelle/polestar/2/1generation/327132/technische-daten.

[69] B. Heibing, S.O. Ersson, Chassis handbook: Fundamentals, driving dynamics, components, mechatronics, perspectives, in: ATZ, Vieweg + Teubner, Wiesbaden, 2011, https://doi.org/10.1007/978-3-8348-9789-3.
[70] Motor Presse Stuttgart GmbH & Co. KG (Ed.), auto motor und sport, Stuttgart.
[71] M. Mitschke, Dynamik der Kraftfahrzeuge, 5., überarb. u. erg. aufl. 2014, Springer Vieweg, Wiesbaden, 2014, https://doi.org/10.1007/978-3-658-05068-9.
[72] U. Peckelsen, Objective Tyre Development: Definition and Analysis of Tyre Characteristics and Quantification of their Conflicts, in: Karlsruher Schriftenreihe Fahrzeugsystemtechnik / Institut für Fahrzeugsystemtechnik, volume 57, KIT Scientific Publishing, Karlsruhe, 2017, https://doi.org/10.5445/KSP/1000073428.
[73] P. Englert, Knall-effekt? Auto Motor und Sport 2022 (21) (2022) 31–36.
[74] T. Hellmanzik, Der lanzenbrecher, Auto Motor und Sport 2021 (23) (2021) 16–22.
[75] S. Renz, Watt-rund-fahrt, Auto Motor und Sport 2021 (18) (2021) 60–68.
[76] S. Renz, Auf dem weg nach ganz ohm? Auto Motor und Sport 2022 (10) (2022) 12–21.
[77] P. Serra, M. Innocenti, A. Balestrino, Lateral dynamics and control of a 4WD vehicle using sliding modes, IFAC Proc. Vol. 29 (1) (1996) 7957–7962, https://doi.org/10.1016/S1474-6670(17)58973-9.
[78] Y. Cao, S. Tang, C. Li, P. Zhang, Y. Tan, Z. Zhang, J. Li, An optimized EV charging model considering TOU price and SOC curve, IEEE Trans. Smart Grid 3 (1) (2011) 388–393, https://doi.org/10.1109/TSG.2011.2159630.
[79] A. Jossen, W. Weydanz, Moderne Akkumulatoren Richtig Einsetzen, 2. überarbeitete auflage, Cuvillier Verlag, Göttingen, 2019.
[80] EV Database, Tesla model y Long Range Dual Motor, 05.03.2024, https://ev-database.org/car/1182/Tesla-Model-Y-Long-Range-Dual-Motor.
[81] W. Rudschies, Tesla model y: Elon musks kompaktes elektro-suv im adac test, 03.02.2020, https://www.adac.de/rund-ums-fahrzeug/autokatalog/marken-modelle/tesla/tesla-model-y/.
[82] Tesla model y long range charging curve & performance :: evkx.net, 02.03.2024, https://evkx.net/models/tesla/model_y/model_y_long_range/chargingcurve/.
[83] EV Database, Tesla model y long range dual motor, 05.03.2024, https://ev-database.org/car/1619/Tesla-Model-Y-Long-Range-Dual-Motor.
[84] Hyundai, Hyundai ioniq 5, 29.02.2024, https://www.hyundai.com/eu/models/ioniq5.html.
[85] J. Voelcker, Evs explained: charging losses, Car Driver (10.04.2021).https://www.caranddriver.com/features/a36062942/evs-explained-charging-losses/
[86] X. Zhao, Y. Ma, S. Shao, T. Ma, What determines consumers' acceptance of electric vehicles: A survey in Shanghai, China, Energy Econ. 108 (2022) 105805, https://doi.org/10.1016/j.eneco.2021.105805.
[87] PwC, Welches sind die wichtigsten kriterien bei der auswahl ihres neuen elektroautos?, 2023, Accessed on 14.01.2024, https://de-statista-com.eaccess.tum.edu/statistik/daten/studie/1415450/umfrage/umfrage-erwartete-kosten-fuer-den-e-auto-kauf-nach-region/.
[88] E. Helmers, P. Marx, Electric cars: technical characteristics and environmental impacts, Environ. Sci. Europe 24 (2012) 14, https://doi.org/10.1186/2190-4715-24-14.
[89] E. Higueras-Castillo, S. Molinillo, J.A. Coca-Stefaniak, F. Liébana-Cabanillas, Perceived value and customer adoption of electric and hybrid vehicles, Sustainability 11 (18) (2019) 4956, https://doi.org/10.3390/su11184956.
[90] S.H. van Mastrigt, L. Groenesteijn, P. Vink, L.F.M. Kuijt-Evers, Predicting passenger seat comfort and discomfort on the basis of human, context and seat characteristics: a literature review, Ergonomics 60 (7) (2017) 889–911, https://doi.org/10.1080/00140139.2016.1233356.

Nico Rosenberger was born in Aschaffenburg on October 19, 1995, studied Mechanical Engineering at the Technical University of Darmstadt, and earned his Bachelor's and Master's degrees in 2018 and 2021, respectively. Since 2022, he has been employed at the Institute of Automotive Technology (FTM) at the Technical University of Munich (TUM). His primary research interest is the analysis of battery electric vehicle concepts and optimizing electric powertrains

Moritz Fundel was born in Tübingen in 1997, studied Mechanical Engineering at the Technical University of Munich and earned his Bachelor's and Master's degrees in 2020 and 2023, respectively.

Simon Bogdan was born in Aalen in 1998 and earned his Bachelor's degree in Engineering Science at the Technical University of Munich (TUM) in 2022. Since then, he has been studying the Master's program Development, Production and Management in Mechanical Engineering.

Lukas Köning was born in Berlin on February 10, 2001, earned his Bachelor's in Mechanical Engineering in 2022 and currently persues his Master's in Automotive Engineering at the Technical University of Munich (TUM).

Peter Kragt was born in Landshut in 1998, earned his Bachelor's degree in Mechanical Engineering at the Technical University of Munich (TUM) in 2021. Since then he is pursuing his Master's degree in Automotive Engineering.

Moritz Kühberger was born in Munich in 1998 and earned his Bachelor's in Mechanical Engineering at the Technical University of Munich (TUM) in 2021. Currently, he is completing his Master's in Automotive Engineering

Markus Lienkamp was born in 1967, studied Mechanical Engineering at the Technical University of Darmstadt (TUD) and Cornell University, and obtained his doctorate at TUD in 1995. He worked at Volkswagen as part of an international trainee program and took part in a joint venture between Ford and Volkswagen in Portugal. Returning to Germany, he led the brake testing department in the VW commercial vehicle development section in Wolfsburg. He later became head of the "Electronics and Vehicle" research department in Volkswagen AG's Group Research division. Prof. Lienkamp has been the professor of the FTM at TUM since November 2009.